EBioMedicine 50 (2019) 274–289

Contents lists available at ScienceDirect

EBioMedicine

journal homepage: www.elsevier.com/locate/ebiom

Research paper

Human iPSC-derived astrocytes from ALS patients with mutated C9ORF72 show increased oxidative stress and neurotoxicity

Anastasya Birger[a,b], Israel Ben-Dor[a], Miri Ottolenghi[a], Tikva Turetsky[a], Yaniv Gil[a], Sahar Sweetat[b], Liat Perez[b], Vitali Belzer[b], Natania Casden[b], Debora Steiner[a], Michal Izrael[c], Eithan Galun[d], Eva Feldman[e], Oded Behar[b,*], Benjamin Reubinoff[a,*]

[a] The Sidney and Judy Swartz Embryonic Stem Cell Research Center of The Goldyne Savad Institute of Gene Therapy & The Department of Obstetrics & Gynecology, Hadassah University Medical Center, Jerusalem 91120, Israel
[b] Department of Developmental Biology and Cancer Research, Institute of Medical Research Israel-Canada (IMRIC), Faculty of Medicine, The Hebrew University, P. O. Box 12272, 91120 Jerusalem, Israel
[c] Kadimastem Ltd., Sapir 7, Weizmann Science Park, Nes-Ziona, Israel
[d] The Goldyne Savad Institute of Gene Therapy, Hadassah University Medical Center, Jerusalem 91120, Israel
[e] Department of Neurology, University of Michigan, Ann Arbor, MI, USA

ARTICLE INFO

Article History:
Received 26 July 2019
Revised 24 October 2019
Accepted 18 November 2019
Available online 29 November 2019

Keywords:
Amyotrophic lateral sclerosis
iPSC
Astrocytes
Oxidative stress
Neurotoxicity
Senescence

ABSTRACT

Background: Amyotrophic lateral sclerosis (ALS) is a progressive neurodegenerative disease that affects motor neurons (MNs). It was shown that human astrocytes with mutations in genes associated with ALS, like C9orf72 (C9) or SOD1, reduce survival of MNs. Astrocyte toxicity may be related to their dysfunction or the release of neurotoxic factors.

Methods: We used human induced pluripotent stem cell-derived astrocytes from ALS patients carrying C9orf72 mutations and non-affected donors. We utilized these cells to investigate astrocytic induced neuronal toxicity, changes in astrocyte transcription profile as well as changes in secretome profiles.

Findings: We report that C9-mutated astrocytes are toxic to MNs via soluble factors. The toxic effects of astrocytes are positively correlated with the length of astrocyte propagation in culture, consistent with the age-related nature of ALS. We show that C9-mutated astrocytes downregulate the secretion of several antioxidant proteins. In line with these findings, we show increased astrocytic oxidative stress and senescence. Importantly, media conditioned by C9-astrocytes increased oxidative stress in wild type MNs.

Interpretation: Our results suggest that dysfunction of C9-astrocytes leads to oxidative stress of themselves and MNs, which probably contributes to neurodegeneration. Our findings suggest that therapeutic strategies in familial ALS must not only target MNs but also focus on astrocytes to abrogate nervous system injury.

1. Introduction

Amyotrophic lateral sclerosis (ALS) is a late onset incurable neurodegenerative disease, characterized by a progressive loss of motor neurons (MNs) in the cerebral cortex, brainstem, and spinal cord. Nearly 20% of ALS patients have inherited familial ALS (fALS) [1]. To date, genetic aberrations in more than 20 different genes have been identified to cause ALS, including C9orf72 (C9), SOD1, TDP-43 and FUS [2]. The most frequent genetic cause is a hexanucleotide GGGGCC repeat expansion in the C9 gene [3,4]. The remaining 80% of ALS patients have no family history of the disease and are therefore classified as sporadic cases (sALS).

Accumulating evidences suggest that astrocytes play a key role in the pathogenesis of ALS. In healthy individuals, astrocytes play a role in many physiological processes that ensure the wellbeing of neurons in the CNS, including production and delivery of energy metabolites and antioxidants [5,6]. Glutathione metabolism in astrocytes boosts neuronal antioxidant defenses and protects neurons from increased oxidative stress that can result from neurotransmission and metabolic activity [7,8]. Dysregulation of this astrocyte-neuron interplay, key for normal CNS function, is likely to contribute to neuronal death.

Astrocytes carrying mutations in SOD1, C9 and astrocytes derived from sALS patients were found to be toxic to MNs *in vitro* and *in vivo* via a non-cell autonomous pathway [9–15]. Moreover, it was shown that SOD1 and C9-mutated astrocytes were able to decrease the number of MNs via soluble factors [10,11,14,16]. The death of MNs in ALS could result from either a loss of astrocytic support functions and/or the secretion of neurotoxic factors, including cytokines. There are

* Corresponding authors.
E-mail addresses: oded.behar@mail.huji.ac.il, odedb@ekmd.huji.ac.il (O. Behar), BenR@hadassah.org.il (B. Reubinoff).

https://doi.org/10.1016/j.ebiom.2019.11.026

Research in context

Evidence before this study

Evidence before this study: Amyotrophic lateral sclerosis (ALS) is a progressive incurable neurodegenerative disease characterized by the death of motor neurons (MNs). Recent studies have demonstrated that astrocytes from ALS patients, including those with the C9-mutation, are capable of inducting motor neuron death. Astrocyte toxicity has been suggested to be either due to release of neurotoxic factors however, other studies are more consistent with astrocyte dysfunction.

Added value of this study

In this study we showed that induced pluripotent stem cell-derived C9-mutated astrocytes are toxic to MNs via soluble factors, and that the toxicity of C9-mutated astrocytes is positively correlated with the length of culturing. Transcriptional and secretome profiles of astrocytes derived from patients carrying a mutation in the C9 gene indicated the increased frequency of mutated astrocytes to enter senescence and a reduction in the secretion of several antioxidant proteins. As a result, the reactive oxygen species (ROS) level in astrocytes was increased. Furthermore, we demonstrated that conditioned medium collected from C9-mutated astrocytes results in increased oxidative stress in wild type MNs.

Implications of all the available evidence

Our results suggest that MNs vulnerability in ALS patients with C9-mutation is caused in part by C9-astrocytes failure to regulate oxidant levels. Hence, astrocyte dysfunction should probably be considered when developing ALS therapeutics.

controversial data which support each of these possibilities, yet it still remains to be clarified.

Postmortem analyses of spinal cords from ALS patients reveal global oxidative damage in astrocytes, microglia and neurons [17]. At the cellular level, increased reactive oxygen species (ROS), the radicals that mediate oxidative damage, leads to cellular senescence, among other cellular fates including apoptosis, necrosis and autophagy [18]. Cellular senescence is a stable growth arrest phase of cells characterized by the secretion of senescence-associated secretory phenotype (SASP) factors. Senescent cells accumulating in tissues over time result in increased levels of SASP factors that may contribute to the chronic inflammatory environment seen in ALS [reviewed in [18]]. Recently, in a rodent model overexpressing mutant SOD1, it was shown that the rate of astrocytes acquiring a senescent phenotype is accelerated and they subsequently provide less support to MNs [19]. However, whether genetic mutations, like the C9 mutation, in astrocytes increases the tendency for senescence is not yet known.

To better understand the role of astrocytes in familial ALS, we set out to study the properties of patient-induced pluripotent stem cell (iPSC)- derived astrocytes harboring the C9-mutation to uncover potential cellular mechanisms leading to MN death. We combined stem cell-based *in-vitro* modeling with unbiased approaches of screening to identify the transcriptional and functional changes induced by the C9-mutation in astrocytes. We show that C9-mutated astrocytes downregulate the secretion of several antioxidant proteins, and display increased oxidative stress and senescence. We further show increased oxidative stress in MNs cultured in media conditioned by C9-astrocytes. Our findings suggest that dysfunction of C9-astrocytes leads to oxidative stress of themselves and MNs, which probably contributes to neurodegeneration.

2. Methods

2.1. Cell culture

Primary fibroblast cultures of healthy and C9-ALS donors were received from the U-M ALS clinic. Cells were cultured in high-glucose DMEM (Invitrogen) supplemented with 15% fetal calf serum (Biological Industries, Beit Haemek, Israel), 2 mM L-glutamine, 50 U/ml penicillin, and 50 μg/ml streptomycin (all from Invitrogen). iPSC lines were maintained on mitomycin-C (MMC; Sigma-Aldrich, 10 μg/ml)-treated human foreskin fibroblasts in gelatin-coated six-well plates (Nunc, Glostrup, Denmark; 3 × 105 feeders/well) cultured in hESC medium, which consisted of Knockout DMEM supplemented with 16% KnockOut SR, 2 mM L-glutamine, 1% nonessential amino acids, 0.1 mM β-mercaptoethanol, 50 U/ml penicillin, 50 μg/ml streptomycin (all from Invitrogen), and 5 ng/ml bFGF (Peprotech, Rocky Hill, NJ) in a 5% O2 incubator. iPSCs were passaged weekly by mechanical dissection or by dissociation with 1 mg/ml collagenase IV (Gibco). hESC line HB9-GFP [20] and iPSC lines with normal karyotypes were used within passages 21–35. HB9-GFP, carrying GFP under the promoter of HB9 was kindly provided by dr. Kevin Eggan. Colonies of hESC and iPSC were grown on HFF feeder cells in KO-DMEM supplemented with 14% KO serum replacement, 1% nonessential amino acids, 1% glutamine, 0.5% penicillin/streptomycin, 0.1 mM β-mercaptoethanol (all from Gibco-BRL, Carlsbad, CA, USA), and 4 ng/ml of bFGF (Pepro-Tech Rocky Hill, NJ, USA). hESC and iPSC colonies were passaged every 6–7 days manually or using collagenase type IV 1 mg/ml (Gibco-BRL) for 1.5 h/ 37 °C. hESC and iPSC were cultured at 37 °C in 5% CO2 and 5% O2.

2.2. Cell reprogramming and differentiation

Skin fibroblasts reprogramming was carried out by the STEMCCA lentiviral system [21]. Excisable lentivirus containing human OCT4, SOX2, KLF4, and c-MYC transcription factors in a single cassette (pHAGE2-EF1α-hOct4-F2A-hKlf4-IRES-hSox2-P2A-hcMyc-W-loxP) was produced using a five-plasmid transfection system in HEK293T cells [22]. Transfection medium was replaced with fresh medium 24 h post transfection and again 6 h later. Viral supernatant (7 ml per 10-cm dish) was collected 42 and 56 h after transfection and passed through a 0.45 μm filter. The supernatant was used immediately or stored at −80 °C for up to 2 years.

A day before transduction, 8.5×10^4 human skin fibroblasts from control or C9-ALS donors, typically at passage 3 or 4, were plated on a gelatin-coated well of 6-well plate. Transduction was performed with 0.7 ml viral supernatant, 0.7 ml fresh medium and 5 μg/ml polybrene per well. On the next day, the medium was changed to hESC medium and the cells were transferred to 5% O2 incubator. On the sixth day, the cells were trypsinized and plated at a dilution of 1:32 in the presence of 10 μM Y-27,632 in 2 × 10 cm gelatin-coated dishes pre-seeded the day before with MMC-inactivated human foreskin fibroblasts (1.8×10^6 per dish). At day 33–34 post transduction single iPSC colonies were mechanically isolated. Isolated iPSC clones were expanded and seeded on puromycin resistant foreskin fibroblasts [23] and 4–5 days later transiently transfected with the Cre expression plasmid pEFBOS-Cre-IRES-Puro to obtain lines without ectopic reprogramming factors. Transfected cells were selected for two days with 1.7 μg/ml puromycin, starting one-day post transfection. Colonies were picked 14–16 days after transfection and removal of the reprogramming factors was verified by PCR analyses (Table 1, PCR sets 1 & 2). After removal of the reprogramming factors iPSCs still carry a 303 bp fragment of integrated inactive LTR as demonstrated by PCR analysis (Table 1, PCR set 3). Characterization of iPSCs and immunostaining was performed as previously reported [24].

Table 1
Primers for PCR analyses.

PCR set No.	primer target sites (product)	Primers sequences	Product size (bp)	Annealing temp
1	STEMCCA 7194F	5-TACAACTCCATGACCAGCTCG	435	60
	STEMCCA 7628R	5-GTTCCTGTTGGTGAAGCTAACG		
2	STEMCCA 7441F	5-GACTTCACATGTCCCAGCACTAC	498	60
	STEMCCA 7938R	5-AACTCTGGTTCACCATGTCTCC		
3	LTR-F	5-GGCTAATTCACTCCCAACGA	268	57
	LTR-R	5-GGTCTGAGGGATCTCTAGTTACC		

2.3. Generation of spinal cord astrocytes

Differentiation of iPSCs into spinal cord astrocytes was performed using a previously published protocol with slight changes directing neural precursor cells to acquire spinal cord specification [25,26]. Briefly, iPSC colonies were detached from the feeder cells using collagenase type IV, collected, centrifuged and re-suspended in NSCR medium (AdDMEM/F12 supplemented with 1% N2 and 0.1% B27, 1% nonessential amino acids, 1% penicillin/streptomycin, 1% GlutaMAX solution (all from Invitrogen) and distributed into 6–12 low cell attachment well plates to avoid adhesion. For neural induction, NSCR medium was supplemented with 10 μM SB431542 (Biogems, Westlake Village, CA, USA), 2.5 μM Dorsomorphin (Calbiochem) and 0.5 μM N-acetylcysteine (Sigma) for the first 4 days. At day 4, 1 μM retinoic acid (RA, Sigma-Aldrich, St. Louis, MO, USA) was added to medium. At day 7, 500 μM Purmorphamine (Biogems) was added to medium. At day 11 SB431542, Dorsomorphin, retinoic acid, and Purmorphamine were omitted. The neurospheres were mechanically chopped at the beginning of the glial enrichment phase and cultured in NSCR medium with addition of 20 ng/mL leukemia inhibitory factor (LIF) and 20 ng/mL epidermal growth factor (EGF)(PeproTech) for 3 weeks. After enrichment, the spheres were propagated in NSCR medium for 3 weeks. After this, monolayer cultures were generated by dissociating the spheres using Accutase (Gibco-BRL) for 10 min/ 37 °C and single cells or small clumps were plated on plates coated with Matrigel (BD Biosciences; 1:80 dilution). The monolayer of astrocyte precursor cells (APC) cultures were propagated in NSCR medium supplemented with 20 ng/mL EGF, 20 ng/mL basic fibroblast growth factor (bFGF, PeproTech) for 3 weeks and passaged when confluent by using Accutase (Sigma, split ratio 1:2–1:3). Astrocyte populations were obtained by differentiating the APCs for at least 30 days of final differentiation with AstroMED (Neurobasal supplemented with 0.2% B27, 1% nonessential amino acids, 1% penicillin/streptomycin, 1% GlutaMAX solution (all from Invitrogen) with 10 ng/mL ciliary neurotrophic factor (CNTF, PeproTech). Astrocytes were passaged using Try:EDTA solution (1:10) for 2 min to fresh Matrigel every week or two based on confluence. In each of the experiments, the passage number and the time in culture of each line were identical. The passage number in all experiments did not exceed passage 10. All astrocyte lines (C9-mutated and control) went through the same passage scheduling. Until passage 4 all cell lines were split at a ratio of 1:4. A tendency to divide slower with each passage was observed in all lines but was more prominent in the C9-mutated lines. Hence, from passage 5 onward, the split ratio of each line was individualized according to the number of cells that were harvested.

For immunostaining, astrocytes were seeded on cover slips pre-coated with poly-D-lysine (10 μg/ml) and laminin (4 μg/ml). The medium was replaced every 3 days with fresh factors along the whole protocol. Cells were cultured at 37 °C in 5% CO2 and 5% O2.

Conditioned medium preparation for neuronal survival experiments:

Conditioned medium was generated by incubating the astrocytes with neurobasal medium supplemented with 0.2 x B27. Conditioned medium was collected every two days and was used immediately to replace 50% of the neuronal medium every 2 days.

Concentrated conditioned medium experiments:

C9-mutated and control conditioned media was pooled from two control lines and two mutated lines and separately concentrated X10 using Amicon® ultra centrifugal filters with a molecular weight cut-off of 3 kDa. The concentrated medium from both mutated and control lines were added back into control conditioned medium in a ratio of 1 vol of concentrated medium with 9 vol of the non-concreted medium. This reconstituted medium was used to replace 50% of the neuronal medium every 2 days.

2.4. Generation of human spinal MNs

Differentiation of hESC into spinal cord MNs was performed using a previously published protocol with slight changes [20]. Briefly, hESC colonies were detached from the feeder cells using collagenase type IV, collected, centrifuged and gently re-suspended in NSC medium (DMEM:F12 supplemented with B-27 × 1, N2 × 1, 1% nonessential amino acids, 1% glutamine, 0.5% penicillin/streptomycin (all from Gibco-BRL), heparin 1 mg/500 ml) and distributed into 6–12 low cell attachment well plates to avoid adhesion. For neural induction, NSC medium was supplemented with 5 μM SB431542 (Biogems, Westlake Village, CA, USA) and 500 ng/ml Noggin (PeproTech) for the first 6 days. At day 6, SB431542 and Noggin were omitted, and the neural precursor cells were further cultured in NSC medium supplemented with 1 μM retinoic acid (Sigma-Aldrich, St. Louis, MO, USA), 1 μM cAMP (db-cAMP, Sigma), and 5 ng/ml FGF2 (PeproTech) for 3 days and then 500 μM Purmorphamine (Biogems) was added. From day 13 until 25–30 the concentration of retinoic acid and Purmorphamine was reduced to 0.5 μM and 250 μM, respectively. From day 25 to NSC medium were added 10 ng/ml h-BDNF, h-GDNF, h-IGF1 (all from PeproTech) and 10 μM DAPT (Sigma) for at least 5 days. At day 30 the neurospheres were taken to FACS sorting. For immunostaining, neurospheres were dissociated using Accutase (Gibco-BRL) for 0.5 h/ 37 °C and single cells or small clumps were plated on coverslips pre-coated with poly-D-lysine (10 μg/ml) and laminin (4 μg/ml). The medium was replaced every 2 days with fresh factors along the whole protocol. Cells were cultured at 37 °C in 5% CO2 and 5% O2.

2.5. Derivation of mouse cortical neurons

Plates were coated with poly-D-lysine (Sigma P1024) overnight in 37 °C, cortical neurons were isolated from embryo (E16.5). Cortices were dissected out and the hippocampus, meninges and the pia layers were removed. Digestion solution was added to the cortices (digestion with papain (Worthington, #3126) 20units/ml and 2 ml /brain in HBSS) and the samples were incubated for 4 min at 37 °C water bath. Later the digestion solution was removed and the same volume of inhibitor solution was added (inhibitor solution included 1 g trypsin inhibitor (Sigma, T9253) with 1 g BSA for 1 L HBSS+MgCl +Hepes) and the samples were incubated for 2 min at 37 °C water bath. The inhibitor was replaced for three times total. After removal of final inhibitor solution, 5 mL of Neurobasal media (Invitrogen, 21,103–049) with the addition of 1xB27 (Invitrogen, 17,504–044) was added. The tissues were titrated by 1 ml tip 10 times. After 1 min

the supernatant was taken to a new tube and centrifuged for 1 min at 250 g. Then the pellet was suspended with Neurobasal media. The cells were counted and plated on coated plates. For the Alamar blue assay, 40,000 cells per 96 well were used. The medium was changed every 2 days. For the experiments with the conditioned medium, we changed the medium to the conditioned medium the day after the isolation.

2.6. Immunocytochemistry

Cells were fixed in 4% paraformaldehyde (PFA; Sigma, St Louis, MO, USA) at room temperature for 15 min, rinsed with phosphate-buffered saline (PBS), and permeabilized with 0.2% Triton X-100 containing 5% normal donkey serum for 30 min at room temperature. Cells were then labeled with primary antibodies for 2 h at room temperature or overnight at 4 °C with the following conditions: HB9 (1:80, 81.5C10, DSHB), CHAT (1:200, AB144P, Millipore-Merck), Olig2 (1:80, AF2418, R&D), β3-Tubulin (1:1000, T8578, Sigma or MRB-435P-100, Biolegend), Vimentin (1:100, M7020, Dako), S100b (1:200, S2532, Sigma), GFAP (1:200, Z0334, Dako), O4 (1:150, MAB-1326, R&D), NeuN (1:400, D3S3I, Cell Signaling Technology). All antibodies were diluted in PBS containing 5% serum and 0.2% Triton X-100. The cells were washed the following day and incubated with Cy3-, Cy2- and Cy5-conjugated antibodies (Jackson Immunoresearch Laboratories) for double-staining experiments and processed for visualization using standard protocols.

2.7. Glutamate uptake assay

To measure glutamate uptake, astrocytes were seeded 48 h before the test in 80% confluency and then incubated with 50 μM glutamate (G8415, Sigma) in AstroMED for 1 h at 37 °C in triplicate. Media samples were collected after 0.5 and 1 h and glutamate levels were quantified using the Glutamate Assay Kit (Cell Biolabs, Inc. cat. no. STA-674) according to the manufacturer's instructions. Fluorescent reaction product levels were quantified at 590–600 nm using a microplate reader Tecan Infinite F200 PRO and Tecan-i-control software.

2.8. Flow cytometry

Astrocytes were washed with PBS and incubated with Try:EDTA (1:10) for 2 min at 37 °C. The cells were dissociated into single-cells by pipetting, washed with FACS buffer containing PBS, 1% BSA, and 0.1% Sodium-azide and filtered. Astrocytes were stained for 30 min with the primary antibody anti-EAAT1 (1:10, 130–095–814, Miltenyi) or isotype control (1:10, 130–091–836, Miltenyi), EAAT2 (1:25, AB1783, Chemicon) or secondary antibody. For staining with the antibody anti-CD44 (1:10, IQP-118F, IQ Products) or Isotype control (1:10, IQP-193F, IQ Products), astrocytes were previously fixed by 4% paraformaldehyde for 10 min, permeabilized by 0.2% TritonX in PBS for 10 min, washed with FACS buffer and then stained for 30 min. After the staining, the cells were washed with FACS buffer, centrifuged for 5 min/3500 rpm, and re-suspended in FACS buffer. In the case of EAAT2, cells were stained for 30 min with the secondary antibody donkey anti guinea pig Cy5-conjugated (Jackson Immunoresearch Laboratories, Jackson, PA, USA). After secondary antibody staining, the cells were washed with FACS buffer, centrifuged for 5 min/3500 rpm, re-suspended and analyzed. Live cells were gated using propidium iodide (PI, P4170, Sigma).

HB9-GFP hESC-derived MNs were analyzed by GFP signal. Undifferentiated hESC and GFP negative MNs derived from line hES1 were used as negative controls for gating GFP-positive MNs. At least 10,000 live cells were acquired for cell-associated immunoreactivity with the FACS Caliber system (Becton-Dickinson, Immunocytometry Systems) or CytoFlex (Beckman Coulter Life Sciences) and were analyzed with FCS Express 3 (De Novo software) or CytExpert Software (Beckman Coulter Life Sciences).

2.9. FACS sorting

Neurospheres enriched with HB9-GFP MNs were washed with PBS twice and dissociated using papain (20 units/ml, LS003119, Worthington) for 2 min at 37 °C. Equal amount of fetal calf serum (FCS, Gibco) was added to stop papain activity and cells were centrifuged at 1000 rpm for 3 min. Then cells were treated by DNA solution (250 units/ml) for 10 min at 37 °oC. Cells then were washed, centrifuged and resuspended in presorted medium (NSC medium as described in the protocol for MN differentiation with the addition of 1% FCS and factors h-BDNF, h-GDNF, h-IGF1, CNTF (10 ng/ml all from PeproTech) and 1 μM cAMP (db-cAMP, Sigma)) to 5 million cells/ml. Cells were strained through a 70 mm cell strainer (BD Biosciences) and 100 units of DNAse were added to 1.5 ml of cell suspension. Cells were sorted with a FACSAria II (BD Biosciences) with 80 mm nozzle at approximately 20 PSI and were collected in post sorted medium (NSC containing 2% penicillin/streptomycin, 2% FCS, factors as in presorted medium and 2.5ul/ml Rock inhibitor (25 mM, #1,293,823, Biogems). Cells were centrifuged and re-suspended in fresh growth medium containing growth factors for plating on cover slips pre-coated with poly-D-lysine (10 μg/ml) and laminin (4 μg/ml) or on 8-well chambers (#177,445, Thermo Scientific™ Nunc™ Lab-Tek™ Chamber Slide™) pre-coated with laminin (4 μg/ml).

2.10. Alamar blue (AB) assay

The viability of mouse cortical neurons and human motor neurons was tested after 1, 2 and 3 weeks of treatment or after 24hr, 6 and 14 days of treatment, respectively. AB was added directly into culture media at a final concentration of 10% and the plate was returned to the incubator (5% CO2 and 5% O2 in air, at 37 °C). A shift in color of the culture medium from indigo blue to fluorescent pink, due to conversion of oxidized form of the AB into reduced form was measured by fluorescence plate reader. The amount of color formed is proportional to the number of viable cells. Fluorescence intensity of the samples was measured at 580–610 nm. As a negative control, AB was added to naïve medium.

2.11. RNA sequencing

Libraries were prepared from total RNA using 5 PRIME PerfectPure RNA Purification kit (Gentra Systems, Inc.). cDNA libraries were produced according to Illumina TruSeq RNA protocol. Library generation was performed at The Core Research Facility of The Faculty of Medicine, the Hebrew University of Jerusalem. The sequencing was performed at the Technion Genome Center using Illumina HiSeq 2500. All FASTQ files were analyzed using FastQC (version (v0.11.2), trimmed using the FASTX (version 0.0.14), adapter sequences were removed with Trim Galore (version 0.3.7), The remaining reads were further filtered to remove very low-quality reads, using the Fastq Quality Filter program of the FASTX package. The processed fastq files were mapped to the human transcriptome and genome using TopHat (v2.0.13). The genome version was GRCh38, with annotations from Ensembl release 78. Differential expression was done with Cufflinks package (v2.2.1). Significantly differentially expressed genes were defined as ones with at least 0.3 FPKM level of expression in at least one of the conditions and a q-value less than 0.05.

2.12. qPCR analysis

Total RNA was extracted from cells by 5 PRIME PerfectPure RNA Purification kit (Gentra Systems, Inc.). cDNA was synthesized with qScriptTM cDNA Synthesis Kit (Quantabio, Beverly, MA, USA.)

according to the manufacturer instructions. qRT-PCR was performed with PerfeCTa SYBR® Green FastMix (Quantabio) or with TaqMan™ Fast Universal PCR Master Mix (2X, 4,352,042, Applied Biosystems).

Primers used for qPCR (SYBR-Green Real-Time PCR):

Gene name	Primer sense	Primer anti-sense	Product size
PRNP	CTATGAGGAC CGTTACTATCG	TGCTTGATTGTG ATATTGACG	126 bp
BNIP3	TGGACGGAGT AGCTCCAAGA	CTTCCTCAGACT GTGAGCTGT	131 bp
GPX8	GTGAAGGATGC AAAAGGAAG	AAGTGGGATG GTCCAAAC	149 bp

Assays used for qPCR (TaqMan™ Fast Universal PCR, Applied Biosystems):

Gene name	Assay
CDKN1A	Hs00355782_m1
TGFB2	Hs00234244_m1
CDKN2C	Hs00176227_m1
E2F1	Hs00153451_m1
TNFRSF10D	Hs00174664_m1
SERPINE1	Hs01126606_m1
CCL2	Hs00234140_m1
STMN1	Hs01027515_gH
IGF2	Hs04188276_m1
IGFBP3	Hs00365742_g1

2.13. β -gal activity staining

To evaluate b-gal activity astrocytes were seeded 24 h before the test in 70% confluency. Cells were fixed with 0.2% glutaraldehyde (G6257, Sigma) in PBS for 5 min, washed 3 times, and incubated at 37 °C for 3 h in staining solution (pH 6.0, 2% 5-bromo-4-chloro-3-indolyl-β-D-galactopyranoside (X-gal, INA-1758–03–00), 10 mM potassium ferrocyanide (244,023, Sigma), 10 mM ferricyanide (P9387, Sigma), 150 mM sodium chloride (S7653, Sigma) and 1 mM magnesium chloride (M8266, Sigma). After 3 h, cells washed with PBS and nuclei stained with DAPI (4′,6-Diamidino-2-Phenylindole, Dilactate, 1:10,000, D3571, Molecular probes, Invitrogen). Cultures were examined under phase-contrast microscopy, DAPI was detected under fluorescent microscopy.

2.14. Mass spectrometry

Astrocytes were plated at 80% confluency and incubated for 48 h in AstroMED medium as mentioned above with addition of CNTF. Conditioned media were collected and centrifuged at 5000 rpm for 10 min. Upper fraction free of cells was collected and stored at −80 °C. All samples were cleaned up from BSA by running 80 μl on an SDS-PAGE gel and cutting out the BSA band. The gel slices were digested by Trypsin. Samples were analyzed by LC-MS/MS on Q exactive (Thermo) and identified by Maxquant software version 1.5.2.8 *versus* the human uniprot databases and against decoy databases (in order to determine the false discovery rate). Sample preparation and mass spectrometry analysis were performed at Smoler Proteomics Center, Technion. Only proteins that were identified with at least 2 peptides and above were tested for significant differences. Statistical analysis was done using Perseus software (Matthias Mann's lab, Max-Planck Institute). p-value threshold on label-free quantification (LFQ) intensities was set to 0.05 for Student's *t*-test values. Difference threshold on LFQ intensities was set to ±2.6.

2.15. Evaluation concentration of proteins

Astrocyte conditioned media were preserved during toxicity experiments with mouse cortical and human motor neurons. Astrocytes were plated at 80% confluency and incubated for 48 hr in AstroMED medium as mentioned above with addition of CNTF. Conditioned media were collected and centrifuged at 5000 rpm for 10 min. Upper fraction free of cells was collected and stored at −80 °C. SOD1, SOD2, and GSS content was determined by using a commercial pre-coated ELISA kit according to manufacturer's instructions (BMS222, Invitrogen; ab178012, Abcam; SED757Hu, Cloud-Clone Corp, respectively). Total protein concentrations were measured by Bradford's assay for normalization. The protein levels were quantified using a standard curve and the results were expressed in ng/ml.

2.16. Cellular reactive oxygen species detection

To measure cellular ROS in astrocytes, we used DCFDA / H2DCFDA - Cellular Reactive Oxygen Species Detection Assay Kit (ab113851, Abcam). Astrocytes were seeded 24 h before the test in 80% confluency. Then, according to the manufacturer instructions, 25uM cell permeant reagent 2′,7′ –dichlorofluorescin diacetate (DCFDA) was added for 0.5 h. For positive control we used cells treated by 250uM TBHP, for negative control untreated and unstained cells. Astrocytes were elevated by Trypsin:EDTA solution (1:10, all from Gibco) for 2 min in 37 °C. Percentage of ROS positive cells was detected by FACS.

To measure cellular ROS in MNs, we used Cellular Reactive Oxygen Species Detection Assay Kit (Deep Red Fluorescence, ab186029, Abcam). Cell permeant reagent was added to MNs for 30 min, then MNs were elevated using papain solution (20 units/ml, Worthington). Positive and negative controls were performed as described above. Percentage of ROS positive cells was detected by FACS. In both cases live cells were gated using PI.

2.17. Statistical analysis

All experiments were performed at least three times unless otherwise indicated. Data are presented as means ±+ SEM or as data as a range of values. Statistical significance was calculated using SPSS software using Mann-Whitney *U* test for comparison between two groups. *p*-value of <0.05 was considered significant.

3. Results

3.1. Generation and characterization of human iPSC-derived astrocytes

iPSC lines were derived from skin fibroblasts of four unrelated C9-mutated ALS patients and two unrelated healthy individuals matched for age and sex to two of the patients (Supl. Fig. 1a). The iPSCs were derived using an excisable lentiviral vector containing human OCT4, SOX2, KLF4, and c-MYC transcription factors in a single cassette [27]. The iPSCs of each of the lines expressed markers of pluripotent stem cells, had a normal karyotype and could give rise to progeny representing the three germ layers both *in-vitro* and in teratoma tumors *in-vivo* (Supl. Fig. 1b–o).

Next, we generated astrocyte cultures from the four C9-mutated and two control-iPSC lines, using previously published protocols [28,29] with some modifications (Fig. 1a). Initial neuralization was induced by culturing clusters of undifferentiated iPSCs in the presence of dual SMAD signaling inhibitors [30]. The neural precursors that were obtained were directed to acquire ventral spinal cord regional identity by retinoic acid and Purmorphamine [31,32]. The neural precursors were further promoted to obtain astroglial specification by prolonged propagation in the presence of EGF and LIF followed by plating and further culture in the presence of EGF and FGF2. Final differentiation (FD) into astrocytes was induced in the presence of CNTF. Banks of astrocyte progenitors were frozen after 3 weeks of propagation as a monolayer with EGF and FGF2. We confirmed that after thawing, the astrocyte progenitors could differentiate into astrocytes with the same phenotype as non-frozen ones (Supl. Fig. 2a).

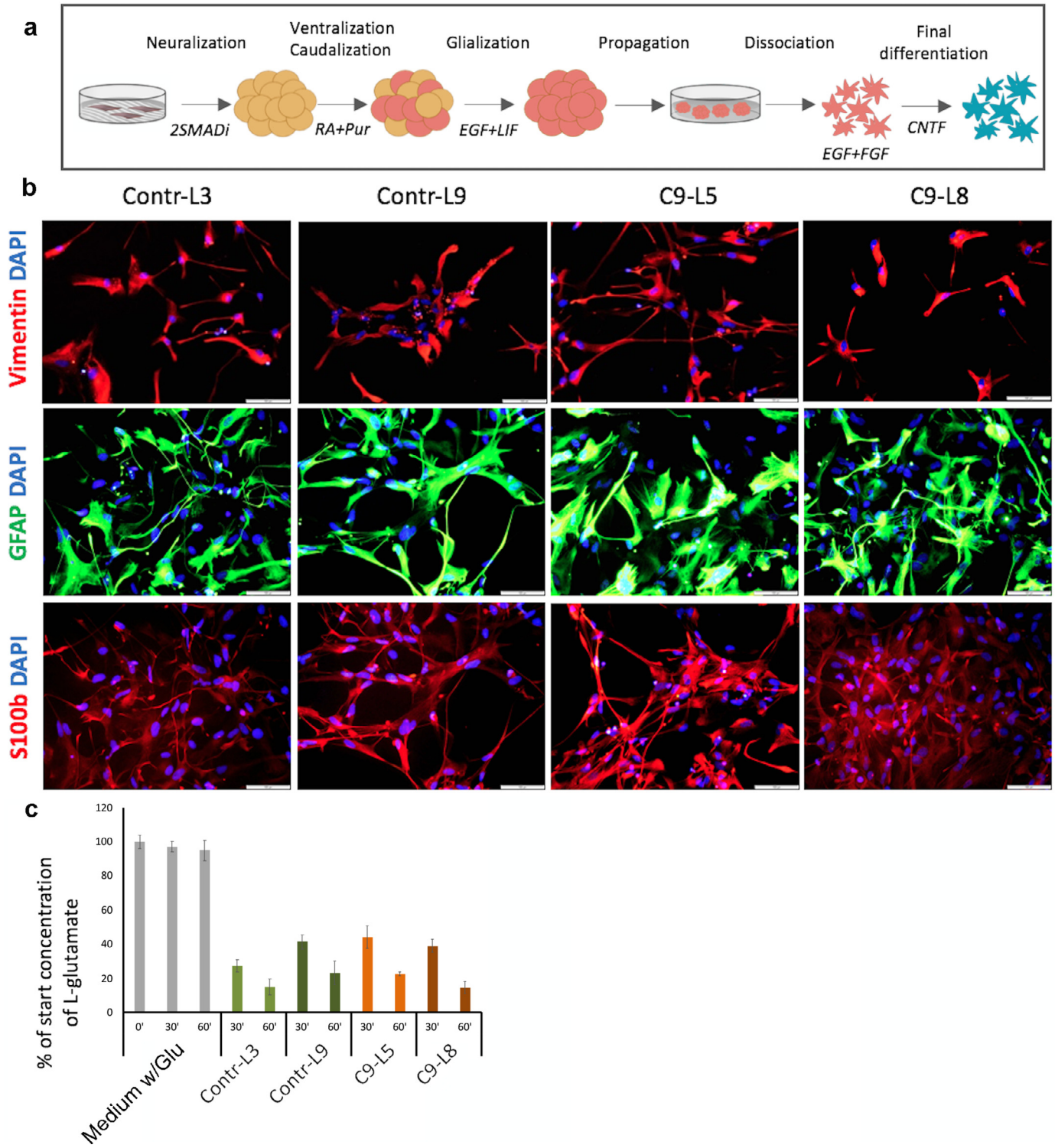

Fig. 1. Generation of functional astrocytes from C9-mutated and control iPSC lines. (a) Schematic presentation of the protocol for induction of astrocyte differentiation. iPSC colonies cultured on feeders were detached for further differentiation as floating spheres in non-adherent plates. Initial neuralization was induced by dual SMAD inhibitors (2SMADi) SB431542 and Dorsomorphin. Further caudalization of the neural progenitor spheres was promoted by retinoic acid (RA) and ventralization by Purmorphamine (Pur). Enrichment for glial progenitors was induced by culture in the presence of epidermal growth factor (EGF) and leukemia inhibitory factor (LIF). The neural spheres were then dissociated, and the cells were plated and further cultured as a monolayer in the presence of EGF and basic fibroblast growth factor (bFGF). Final differentiation to astrocytes was induced in the presence of ciliary neurotrophic factor (CNTF). Please see details in the Methods. (b) Representative immunofluorescence images of C9-mutated (C9-L5, C9-L8) and control (Contr-L3, Contr-L9) astrocytes decorated with anti-Vimentin (red), glial fibrillary acid protein, (GFAP; green), S100β (green) at day 30 of final differentiation (dFD). Nuclei (blue) are counter-stained with DAPI. Scale bars: 100 μm. These experiments were repeated 5 independent times with similar results. c. Histogram presentation of glutamate uptake assay showing that control (Contr-L3, Contr-L9, green bars) and mutated (C9-L5, C9-L8, orange bars) astrocytes uptake L-glutamate from the media at the same rate after 30 and 60 min. The results are normalized to the initial concentration of L-glutamate (50 μM). Data are represented as mean ± SEM of 3 independent experiments with astrocytes at 30–40 dFD. (For interpretation of the references to colour in this figure legend, the reader is referred to the web version of this article.)

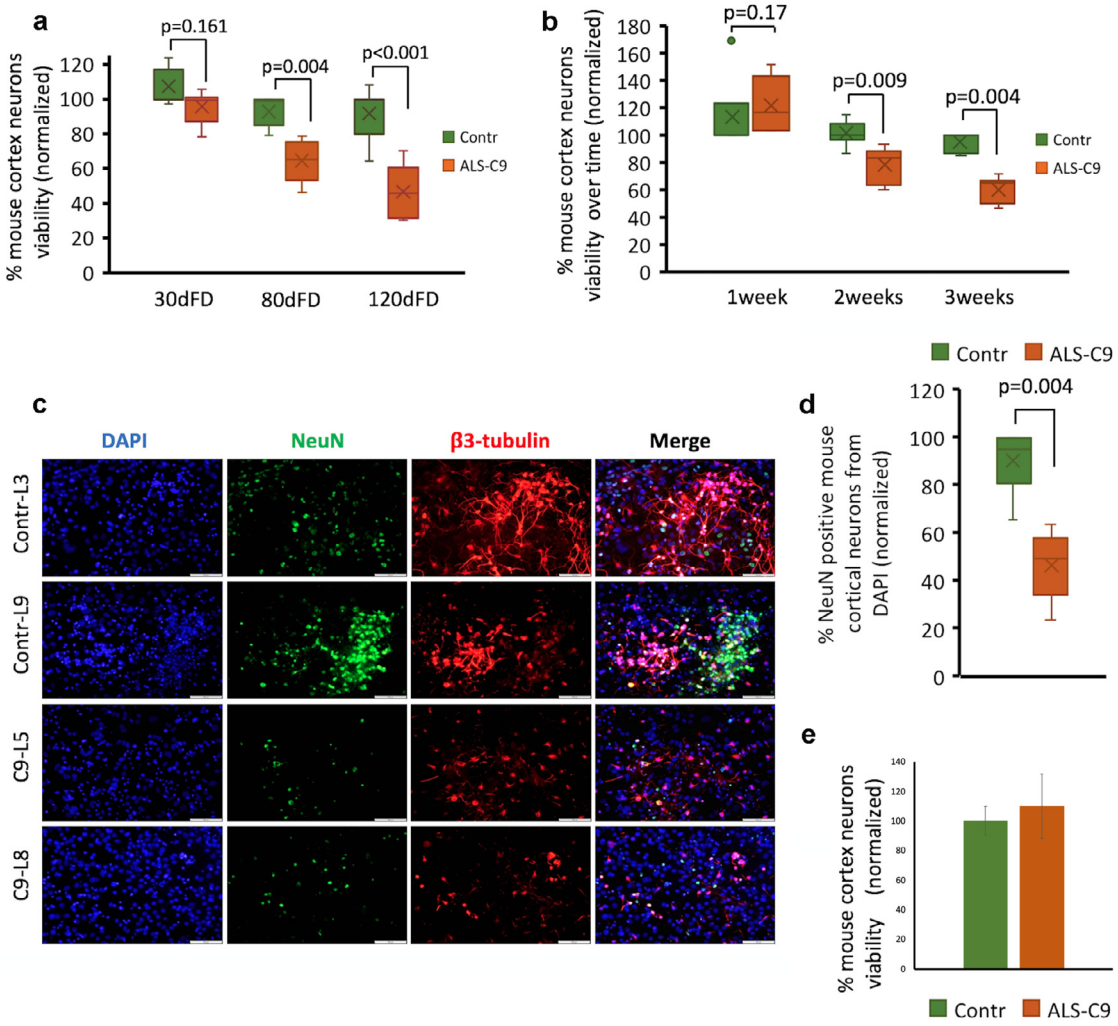

Fig. 2. Toxicity to neurons of media conditioned by C9-mutated astrocytes - its dependence on the astrocyte age in culture. (a) Alamar blue cell viability analysis of mouse cortical neurons showing the toxic effect of media conditioned by C9-mutated astrocytes at 30, 80 and 120 dFD (orange boxes) compared with media conditioned by non-mutated astrocytes (green boxes). Neuronal viability was evaluated after 3 weeks' culture in the conditioned media. Data are represented as a range of values from 3 independent experiments for each time point normalized to Contr-L3 (independent derivations of mouse cortical neurons for each experiment). (b) Analysis of mouse cortical neuron viability was performed as in (a) using media conditioned by C9-mutated (orange boxes) and control (green boxes) astrocytes at 80 dFD. Cell viability was assayed weekly during 3 weeks of culture in the conditioned media. (The data represent 3 independent experiments. Mouse cortical neurons were independently derived for each experiment). (c) Representative fluorescence images of mouse cortical neurons co-immunostained for NeuN (green) and β3-tubulin (red) after 3 weeks of culture in media conditioned by astrocytes at 80 dFD treatment. Nuclei were counterstained by DAPI (blue). Scale bar: 100 μm. (d) Quantitative analysis of the percentage of cells immunoreactive with anti-NeuN after 3 weeks of culture in media conditioned by astrocytes. 16 fields were scored from each condition (n = =3). Data are represented as a range of values from 3 experiments normalized to Contr-L3 (independent derivations of mouse cortical neurons for each experiment). e. Analysis of mouse cortical neuron viability after incubation in C9-astrocyte conditioned medium that was concentrated and further diluted in control medium. Astrocytes at 80 dFD were used to prepare the conditioned medium. Conditioned media pooled from two control (C-L3, C-L9) and pooled from two mutated C9 lines (C9-L5, C9-L8) were concentrated 10-fold. The concentrated media were diluted back into non-mutated astrocytes-conditioned media. These reconstituted conditioned media were used for testing mouse cortical neuron viability as in (a). (For interpretation of the references to colour in this figure legend, the reader is referred to the web version of this article.)

To determine whether the phenotype of C9-mutated astrocytes was different from wild type astrocytes, each iPSC line was differentiated toward astrocyte cultures and the cells were characterized at day 30 of FD for the expression of astroglial markers. Analysis of the expression of Vimentin, S100B and GFAP by immunostaining showed that the majority of cells in all lines expressed these markers (Fig. 1b and Supl. Fig. 2b and c). Flow cytometry analysis of CD44, EAAT1 and EAAT2 expression showed similar rates of expression by astrocyte cultures from all lines (86–92%, 77–94%, 37–55% respectively; Supl. Fig. 2d–f). To further evaluate the purity of cultures of wild type and C9-mutated astrocytes, the cultures were immunostained for non-astroglial lineage markers, including NeuN and O4 for the neuronal and the oligodendroglial lineages, respectively. Less than 0.5% of the cells expressed these non-astroglial markers (Supl. Fig. 2g). Taken together, these results indicated similar high efficiencies of astrocyte differentiation in C9-mutated and control iPSC lines as well as similar astrocytic phenotypes.

We next evaluated the function of wild type and C9-mutated astrocytes. One critical function of astrocytes is buffering of neurotransmitters released during neuronal excitation. To determine whether iPSC-derived astrocytes were functional, we tested the ability of astrocytes to uptake L-glutamate from the medium at day 30 of FD. No significant difference was observed in the L-glutamate clearance properties of C9-mutated and control astrocytes after 30 and 60 min (Fig. 1c).

3.2. iPSC-derived C9-mutated astrocytes toxicity to mouse cortical neurons is positively correlated with the length of astrocyte propagation in culture

Previous studies demonstrated that both fALS and sALS patient-derived astrocytes were toxic to MNs in co-culture systems [15,16]. Furthermore, toxicity was mediated via media conditioned by these

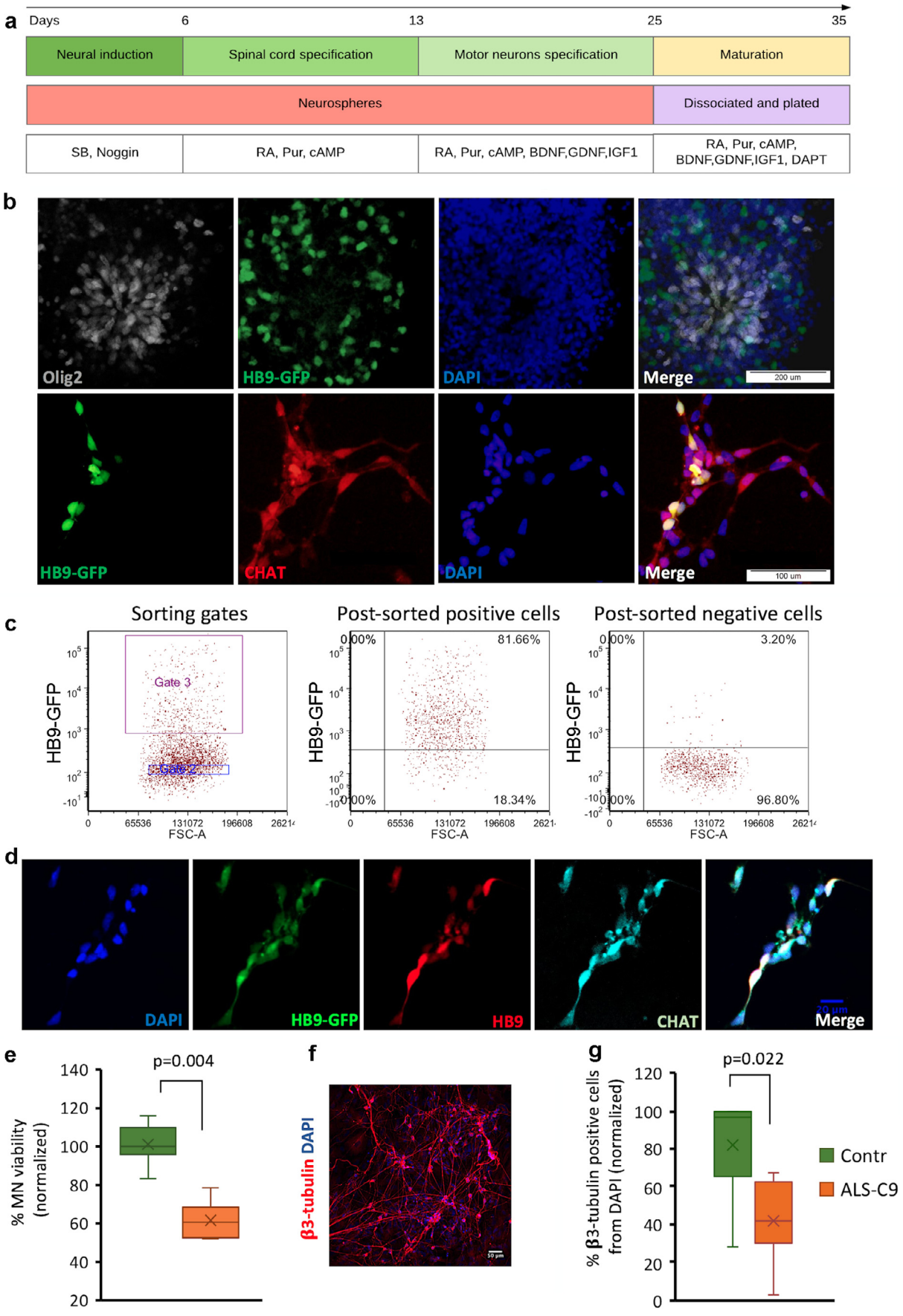

Fig. 3. Toxicity of media conditioned by C9-mutated astrocytes to human iPSC-derived motor neurons. (a) Schematic presentation of the protocol of induction of differentiation of hESC into MNs. (b) Immunostaining of hESC-derived spinal cord MNs showing the expression of the early MN markers Olig2 (white) and GFP under the promoter of HB9 (HB9-GFP)

astrocytes [10,11,14,16]. Given these studies, we next evaluated whether the C9-mutated iPSC-derived astrocytes recapitulated these reported toxic effects, and whether toxicity required physical contact or was mediated by soluble factors.

To address these issues, we derived primary mouse cortical neurons, a cell population that is affected in ALS [33,34]. Since ALS is an age-related disorder, we maintained mouse cortical neurons in media conditioned from C9-mutated and control astrocytes at different time points along FD [30, 80 and 120 days of FD (dFD)]. Neuronal viability was tested every week for 3 weeks. After 3 weeks, there was no discernable difference in the viability of cortical neurons cultured in media conditioned by C9-mutated or control astrocytes at 30 dFD. In contrast, there was a highly significant reduction ($p < 0.001$) in the viability of neurons when they were cultured in media conditioned by 80 dFD C9-mutated compared with control astrocytes. This toxic effect became even more evident when the media was conditioned by astrocytes at 120 dFD (Fig. 2a, data for each line in Supl. Fig. 3a). To test if control astrocytes also provide less support for cortical neurons with age in culture, we compared control astrocytes at 50 and 120 dFD (Supl. Fig 3b). Indeed, astrocytes tended to be less supportive with age in culture, although the difference was not statistically significant.

To further characterize the effect of time in culture on the toxic effect of C9-astrocyte conditioned media, the viability of cortical neurons was analyzed after 1, 2 and 3 weeks of culture in media conditioned by astrocytes at day 80 of FD. After 1 week, there was no significant difference in the viability of cortical neurons cultured in media conditioned by C9 or control astrocytes. However, at both 2 and 3 weeks there was a significant decrease in the viability of neurons cultured in media conditioned by C9-mutated astrocytes (Fig. 2b, data of each line in Supl. Fig. 3c). We verified this result by immunostaining of the neuronal cultures after 3 weeks of cultivation in astrocyte conditioned media for the neuronal markers NeuN and β3-tubulin (Fig. 2c). Quantitative analysis of NeuN-expressing cells confirmed the significant reduction in the percentage (Fig. 2d; data of each line in Supl. Fig. 3d) and the number of neurons per microscopic field (Supl Fig. 3e) after culture in media conditioned by C9-astrocytes. These results suggest that C9-mutated astrocytes are toxic to neurons and reduce neuronal survival via soluble factors. Importantly, this toxic effect is dependent on the age of astrocytes in culture, which is consistent with the nature of ALS as an age-related disease.

The toxic effect of C9-mutated astrocyte conditioned medium could be the result of secretion of toxic factors, or alternatively a reduced capability to support the survival of neurons. To differentiate between these two options we concentrated 10-fold the conditioned media from two pulled C9-mutated astrocytic lines and two pulled control lines. These concentrated media were diluted (1:10) into medium conditioned by control astrocytes. The reconstituted C9-medium was not toxic to cortical neurons (Fig 2e). This result suggests a loss of supportive function rather than toxicity of C9-mutated astrocytic medium.

3.3. iPSC-derived C9 mutated-astrocytes are toxic to human ESC-derived motor neurons

In order to determine the effect of astrocytic conditioned media on human motor neurons (MNs), we generated spinal MNs from human embryonic stem cells (hESC) using a previously published protocol (Fig. 3a, [32,35,36]. We used a hESC line reporting GFP under the control of the promoter of the MN-specific transcription factor HB9, kindly provided by K. Eggan. The hESC HB9-GFP line was differentiated to MNs as described in Fig. 3a and the "Methods" section. The progression of differentiation was monitored at two time points by immunostaining for the MN markers Olig2, HB9 and Choline O-Acetyltransferase (CHAT). At day 15 of differentiation, at the stage of MN specification, we demonstrated cells expressing Olig2, an early MN progenitor marker, as well as cells expressing HB9, an early marker of spinal MNs (Fig. 3b, upper panel). At day 30 of differentiation, at the stage of MN maturation, cells expressing HB9 and the more mature marker CHAT were observed (Fig. 3b, lower panel). The percentage of HB9-GFP positive cells in MN cultures at day 25 was typically 5–10%.

To enrich the cultures for MNs, they were sorted by FACS at day 25 on the basis of GFP expression. FACS analysis of the pre and post-sorted cells showed that 82±5% of the positive post-sorted cells expressed GFP (Fig. 3c), indicating high enrichment for MNs. Immunostaining of post-sorted MNs for HB9 and CHAT showed that the majority of the sorted cells co-expressed these markers (Fig. 3d).

Twenty four hours after sorting and plating, the human MN cultures were fed with media conditioned by C9-mutated and control astrocytes at day 80 of FD. MN survival was monitored by using the Alamar blue cell viability assay. In comparison to mouse cortical neurons, human MNs were more sensitive to media conditioned by C9-mutated astrocytes. A significant toxic effect was detected at 6 days and became more significant after 2 weeks in culture (Fig. 3e, a time dependent effect for each line is presented in Supl. Fig. 4a). This result was confirmed by immunostaining the MNs for β3-tubulin after 2 weeks in culture in the presence of the conditioned media (Fig. 3f and g and Supl. Fig. 4b and c). These results suggest that human C9-astrocytes reduce the survival of human MNs via one or more soluble factors, and the deleterious effects of these factors increase over time.

3.4. Transcriptome analysis of iPSC derived C9-mutated astrocytes

To shed light on the potential mechanism by which C9-mutated astrocytes reduce the survival of MNs, we compared the transcriptome of C9-mutated astrocytes to control astrocytes. RNA-seq analysis was performed on two C9-mutated and two control lines of astrocytes at 80 dFD, a stage at which the C9-mutated astrocytes are toxic to MNs. Whole transcriptome analysis revealed significant homogeneity between the two C9-mutated astrocyte lines, while the two control astrocyte lines exhibited some variability. C9orf72 gene was expressed by all lines. Eight hundred and ninety-nine genes were found to be significantly differentially expressed between control and C9-mutated astrocytes (statistical significance cutoff was $p = 0.05$). Four hundred and fifty genes were up-regulated in C9-mutated astrocytes while 449 genes were down-regulated compared to the controls (Fig. 4a).

To identify signaling and metabolic pathways enriched in C9-mutated astrocytes, we performed gene set enrichment analysis using the Reactome pathway database (https://reactome.org). Analysis of differentially expressed genes revealed enrichment for genes

at day 15 of the differentiation protocol (upper panel, scale bars: 200 μm). Co-expression of HB9-GFP and the mature MN marker CHAT (red) is shown at day 30 of MN differentiation (lower panel, scale bars: 100 μm). Nuclei were counterstained with DAPI (blue). The experiment was repeated 3 times with similar results. (c) HB9-GFP expressing MNs were sorted by GFP signal by Aria II BD FACS sorter. Dot plots present sorting gates and post-sorting analysis. (d) Fluorescence images of sorted MNs after plating and 6 days in culture. The MNs express HB9-GFP (green), and are immunoreactive with both anti-HB9 (red) and anti-CHAT (cyan). Nuclei (blue) are counterstained with DAPI. Scale bar: 20 μm. (e) Alamar blue viability analysis of sorted human MNs after 2 weeks in culture in media conditioned by C9-mutated astrocytes (orange box) and non-mutated astrocytes (green box) at 80–90dFD. Data are presented as a range of values from 3 independent experiments normalized to Contr-L3 (independent derivations of MNs for each experiment). (f) Representative fluorescence image of sorted MNs immunostained for β3-tubulin after 2 weeks in culture in media conditioned by C9-mutated astrocytes. Scale bar: 50 μm. g. Immunostaining analysis of the percent of β3-tubulin-expressing cells from total DAPI+ nuclei within cultures of sorted MNs after 2 weeks in culture in media conditioned by C9-mutated (orange box) and non-mutated (green box) astrocytes. 10 fields were scored per each media condition in each experiment. Data are presented as a range of values from 3 independent experiments normalized to Contr-L3 (independent derivations of MNs for each experiment). (For interpretation of the references to colour in this figure legend, the reader is referred to the web version of this article.)

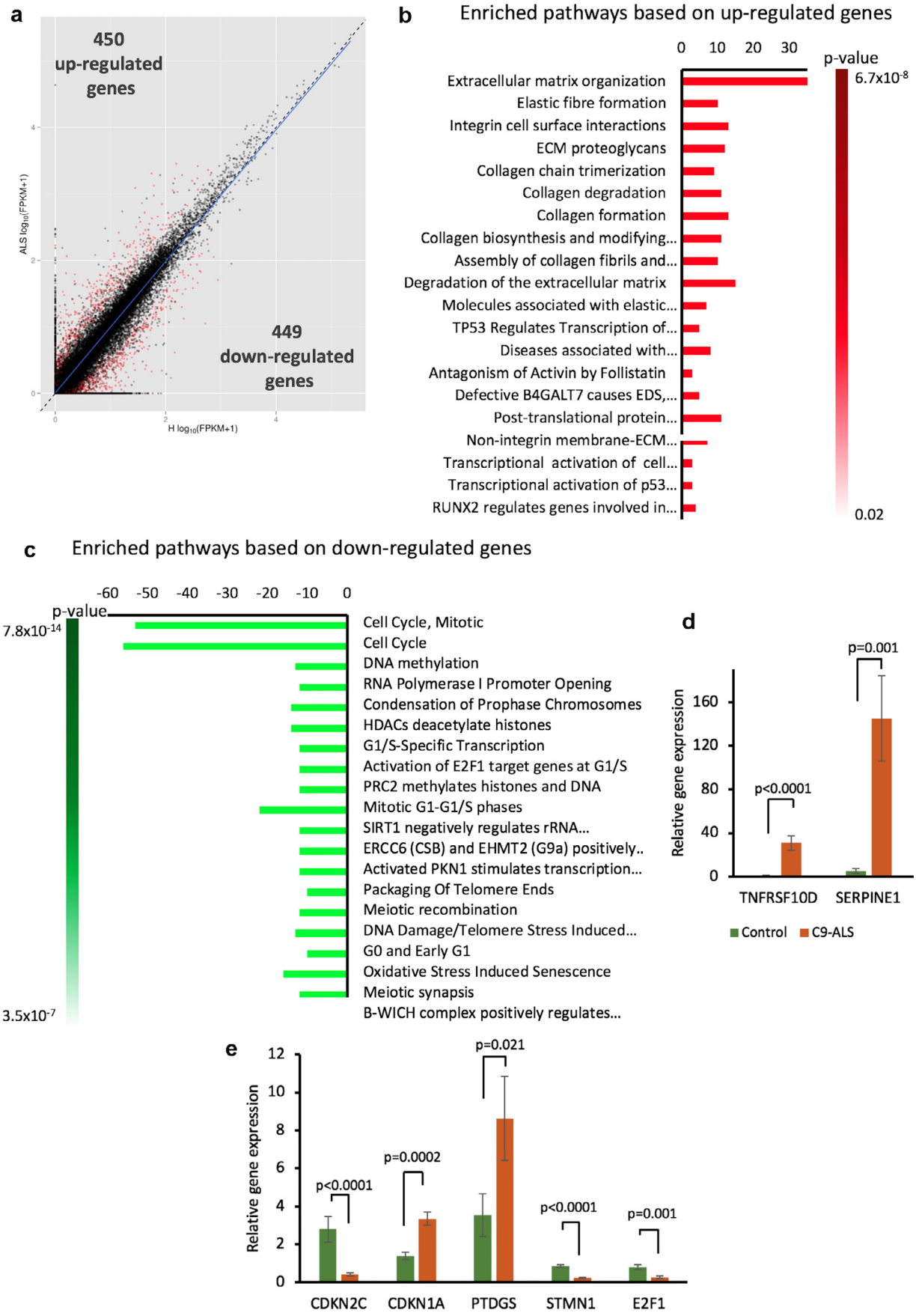

Fig. 4. Transcriptome analysis of C9-mutated and non-mutated astrocytes derived from iPSC. (a) RNA-seq analysis was performed on two C9-mutated (C9-L5, C9-L8) and two unmutated (Contr-L3, Contr-L9) astrocyte lines. Scatter plot of gene expression expressed as log10 (FPKM + +1). Each dot represents a gene. Genes displaying a variability of expression above the specified cut-off (*q*value <0.05, FPKM >0.03 in at least one of the conditions) were defined as differentially expressed and are shown in red. (H, healthy non-mutated

involved in the inhibition of cell cycle and activation of cellular senescence pathways (Fig. 4b). Enrichment for pathways that alter the organization of extracellular matrix was also observed (Fig. 4c). These pathways are associated with the senescence phenotype [37]. We further performed qRT-PCR to validate the different expression of several of the genes related to senescence that were identified by RNA-Seq. For this purpose, we extracted RNA from two control astrocyte and four C9-mutated astrocyte lines (Fig. 4d–e). Gene expression analysis by qRT-PCR verified the altered expression of senescence-associated genes.

3.5. iPSC-derived C9-mutated astrocytes acquire a senescence phenotype

Human astrocytes are highly susceptible to stress and undergo senescent arrest following cellular damage [18,38]. Base on the transcriptomic finding that astrocytes are cell cycle arrested (Fig 4), we sought to determine whether C9-mutated astrocytes undergo senescence in culture at an accelerated rate compared to wild-type astrocytes. We found a significant increase of senescence-associated β-galactosidase (SA β -gal) activity in C9-mutated astrocytes compared to control astrocytes at 90 dFD (Fig. 5a and b, detailed data for each line in Supl. Fig. 5a). Immunostaining of astrocyte cultures for cell cycle markers also revealed high levels of p21 and low levels of Ki67 in C9-mutated astrocytes compared to control cultures (Fig. 5c–e). These data suggest that C9-astrocytes acquire a senescent phenotype at an accelerated rate as compared to control astrocytes.

3.6. Analysis of iPSC-derived C9-mutated astrocytes secretome

Given our results that C9-mutated astrocytes reduce the viability of neurons via soluble factors, we sought to identify the toxic compounds in media conditioned by these cells. We analyzed by mass spectrometry three biological replicates of media conditioned by two C9-mutated and two control astrocyte lines at 70–80 dFD. The conditioned media that were analyzed were shown to be toxic. A total of 1004 proteins were identified. Seventy-one proteins were differentially regulated, of which most (67) were down-regulated and only four proteins were up-regulated in the secretome of C9-mutated astrocytes compared to controls (Fig. 6a). The up-regulated proteins were extracellular matrix proteins including collagen, lumican, olfactomedin-like protein 3 and protein-lysine 6-oxidase, a protein that initiates crosslinking of collagens and elastin. Interestingly, among the down-regulated proteins, several antioxidants were identified including SOD1, SOD2 and GSS (Fig. 6b). We confirmed this result using an ELISA assay for analysis of media conditioned by two control and four C9-mutated astrocyte lines (Fig. 6c–e). Our data show that C9-mutated astrocytes are deficient in producing and/or releasing proteins, including antioxidants, which may make astrocytes more susceptible to oxidative damage, as well effect the viability of MNs cultured in their conditioned medium.

3.7. Oxidative stress in iPSC-derived C9-mutated astrocytes

Deficiency of antioxidants such as SOD1, SOD2 and GSS may lead to diminished defense against ROS, and to increased oxidative stress [18,38]. We therefore measured ROS in control and C9-mutated astrocytes at different ages in culture using a ROS detection assay. Confocal microscopy demonstrated that ROS-positive astrocytes were more abundant among C9 mutated astrocytes at 90 dFD (Fig. 7a). FACS analysis showed that there was no difference in the relative proportion of ROS-positive astrocytes when comparing C9-mutated and control astrocytes at 30 dFD. In contrast, by 80 dFD the relative proportion of ROS-positive C9-mutated astrocyte cells was significantly higher compared to control astrocytes. At 120 dFD, the difference was even greater (Fig. 7b, detailed data for each line in Supl. Fig. 6a).

We further confirmed oxidative stress in C9-mutated astrocytes by analyzing the expression of *GPX8, BNIP3*, and *PRNP* genes that are up-regulated under oxidant stress [39–41]. qPCR analysis showed that C9-mutated astrocytes up-regulated the gene expression of *GPX8, BNIP3*, and *PRNP* compared to control astrocytes (Fig. 7c). These results suggest that reduced production and/or secretion of antioxidants by C9-mutated astrocytes lead to increased oxidative stress within them.

3.8. Oxidative stress in human MNs cultured in medium conditioned by C9-astrocytes

MNs are highly susceptible to oxidative stress [42]. Having established that C9-mutated conditioned media has reduced antioxidant capacity, we asked whether human MNs treated by this media would be more susceptible to oxidative stress. Purified human HB9-reporter MNs were cultured 8 days in media conditioned by C9-mutated and control astrocytes (at 70–90 dFD). The percent of ROS-positive MNs were quantitated from the fraction of GFP-positive MNs (Fig. 7d). MNs cultured in C9-mutated astrocyte-conditioned media had a significantly higher percentage of ROS-positive MNs compared to MNs cultured in control-conditioned media. These data suggest that deficiency of antioxidants in C9-mutated astrocyte-conditioned media leads to oxidative stress in MNs and consequently may contribute to neuronal death.

4. Discussion

In this study, we sought to explore the role of astrocytes in ALS, focusing on the C9orf72-fALS mutation. To that end, we generated astrocytes from human C9-mutated and control-iPSC lines and studied their properties. We found that C9-mutated astrocytes exhibit a non-cell autonomous toxicity to MNs as well as cortical neurons. This toxicity is mediated via soluble factors and does not require contact between astrocytes and MNs. Our findings are consistent with previous studies showing that mouse and human astrocytes bearing ALS mutations, including the C9-mutation, reduce the number of MNs *in vitro* via diffusible factors [10–12,14–16]. Our study further showed that the toxicity of C9-mutated astrocytes increased over time. Media from newly cultured C9-astrocytes showed no toxicity while media from astrocytes cultured from 30 to 120 days revealed increased toxicity over time. Consistent with our data, aged rodent astrocytes have a reduced ability to support MNs compared to young astrocytes, and this effect is more pronounced in astrocytes carrying a mutated SOD1 [19]. ALS is an age-related disease and in cases of fALS, where individuals are born with the causal mutation, disease onset typically does not occur until an older age. Although there are significant differences between age-dependent progression of C9-ALS and prolonged culture conditions of C9-mutated astrocytes, it seems that this experimental system may provide some insight into the age-dependent pathological processes in C9-ALS.

Despite decades of research the nature of astrocyte toxicity in ALS remains unclear. Studies with SOD1 ALS rodents suggest several

lines; ALS, C9-mutated lines). (b and c) The most altered pathways were identified by analysis of upregulated and downregulated genes respectively using the Reactome database. X axis represents number of genes in a pathway. Gradient column represents the significance of recognized pathways. (d and e) qRT-PCR was used to validate the differential expression of selected genes observed by RNA-seq. Validation was performed on RNA from four C9-mutated (C9-L5, C9-L8, C9-L1, C9-L37) and two unmutated (Contr-L3, Contr-L9) astrocyte lines. Data are presented as mean ± SEM of 3 independent experiments (independent differentiations of astrocytes and RNA extractions for each experiment).

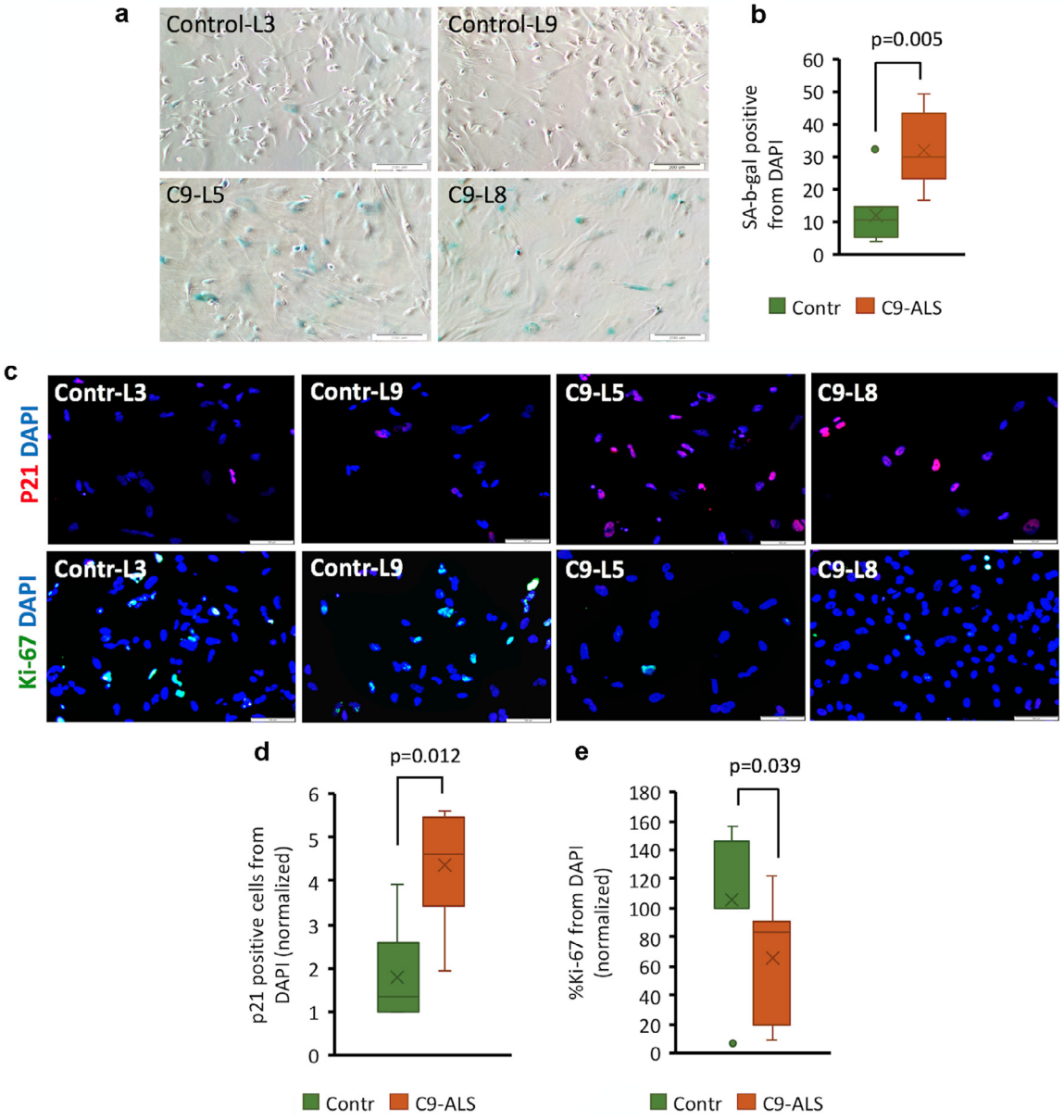

Fig. 5. C9 mutated astrocytes acquire senescence phenotype at higher rates than non-mutated astrocytes. (a) Representative phase-contrast images of mutated (C9-L5, C9-L8) and control (Contr-L3, Contr-L9) astrocytes stained for Sa-β-gal activity. Four independent experiments were performed at 90–100 dFD. Scale bar: 200 μm. (b) Percentage of Sa-β-gal positive astrocytes within C9-mutated (C9-L5, C9-L8, orange box) and control (Contr-L3, Contr-L9, green box) cultures. Ten fields were quantified from each condition. Results are expressed as the percentage of Sa-β-gal positive cells from DAPI counterstained and nuclei normalized to Contr-L3. Data are presented as a range of values from 4 independent experiments (independent differentiations of astrocytes for each experiment). (c) Representative images of C9-mutated (C9-L5, C9-L8) and control (Contr-L3, Contr-L9) astrocytes immunostained for p21 (red, upper panel) and Ki-67 (green, lower panel). Nuclei are counterstained with DAPI (blue). Experiments were performed at 90–100 dFD. Scale bars: 100 μm. D-e. Percentage of p21- and Ki-67-positive cells. Ten fields with about 40 cells per field of immunostained cultures (shown in C) were scored per each condition for the percentage of p21- and Ki-67- positive cells from DAPI normalized to Contr-L3. Data are presented as a range of values from 3 experiments. (For interpretation of the references to colour in this figure legend, the reader is referred to the web version of this article.)

mechanisms including astrocytic mitochondrial dysfunction, altered connexin 43 expression, decreased lactate release, increased nitric oxide production, and increased pro-nerve growth factor (proNGF) secretion [43–46]. These data support the idea that astrocyte-mediated injury in ALS is secondary to a loss of normal astrocytic function and/or a gain of toxic astrocytic function with the production of injurious soluble factors. In the current study, we sought to understand the mechanism(s) underlying astrocyte toxicity in C9-ALS by quantitating the secretome profile of C9-mutated astrocytes. Our findings are more consistent with a loss of function model. First, concentrated C9-mutated conditioned medium diluted in medium conditioned by control astrocytes, no longer show toxicity. Thus, although most molecules in the reconstituted medium retained their original concentration, this medium lost its toxicity. Second, overall more proteins were down-regulated in the secretome of C9-astrocytes compared to control astrocytes. Interestingly, this reduction in protein secretion is in line with recent studies showing an impairment in vesicle secretion in C9-patient-derived neurons and astrocytes [47,48]. Third, consistent with a loss of function model, we observed, reduced levels of important antioxidants such as GSS, SOD1, SOD2 and PRDXs among the down-regulated proteins. In line with this finding, we also observed elevated oxidative stress in C9-mutated compared to control astrocytes. Importantly, the increased oxidative stress of astrocytes was dependent on their age in culture, further supporting the contention that our *in vitro* system may serve as a useful model of the

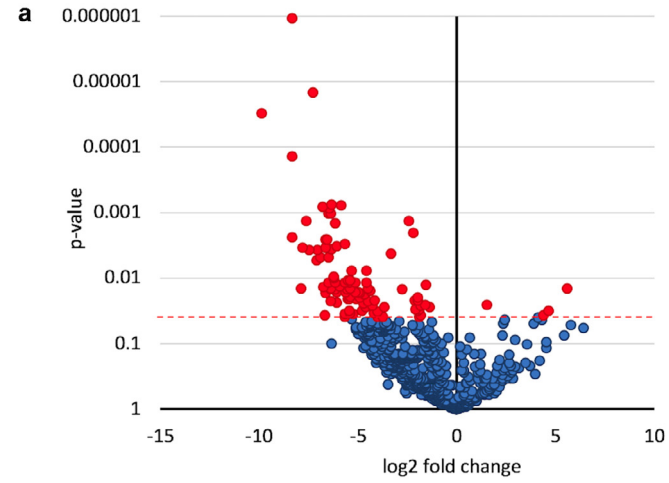

b

Protein name	Gene name	fold change (log2)	p-value
Superoxide dismutase 1	SOD1	-6.07	0.0163
Superoxide dismutase 2	SOD2	-4.95	0.0164
Glutathione synthetase	GSS	-5.24	0.0359

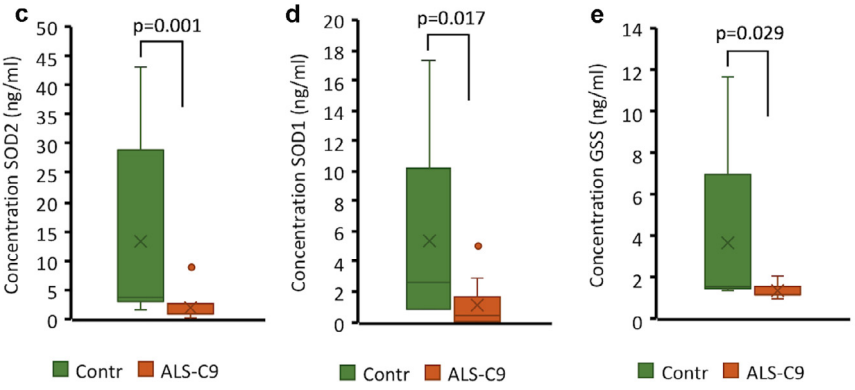

Fig. 6. Secretome analysis of C9 mutated astrocytes. a. Mass spectrometry analysis of control (Contr-L3, Contr-L9) and C9-mutated (C9-L5, C9-L8) astrocyte secretome. 3 biological replicates of media conditioned by each line were analyzed. Conditioned media was collected during toxicity experiments at 70–90 dFD of astrocytes. The results are presented by a volcano plot where each point represents an identified protein. The log2 difference intensity is plotted against the *t*-test *p*-value for each protein. The proteins with significantly ($p < 0.05$) different levels between C9- and non-mutated secretome samples are in red. b. Proteins related to oxidative stress were significantly down-regulated in the C9-mutated secretome. (c–e) Down-regulation of SOD1, SOD2, and GSS in the C9-mutated secretome was validated by ELISA. 3 biological replicates of conditioned media from C9-mutated (C9-L5, C9-L8) and control (Contr-L3, Contr-L9) astrocytes were analyzed by ELISA assay. Data are presented as a range of values from 3 independent experiments.

human condition and may allow for much needed mechanistic studies of fALS.

In the current study, we also discovered that the reduced antioxidant production of C9-astrocytes can adversely affect MN wellbeing. Indeed, we observed increased oxidative stress in wild type MNs that were cultured in C9-astrocytic conditioned media. In agreement with our results, Lopez-Gonzalez and colleagues also reported oxidative stress in C9-mutated MNs derived from iPSCs, that increased as the MNs aged in culture [49]. Collectively, the results from Lopez-Gonzalez et al. and our own data suggest that C9-mutated MNs may undergo oxidative damage as a result of both autonomous (MNs) and non-autonomous (astrocytic) dysfunction. Thus, over time, MNs in C9-ALS patients are exposed to increasing levels of oxidants.

Oxidative stress has been suggested to contribute to the death of MN. For instance, conditioned media derived from mouse astrocytes expressing mutated SOD1 or TDP43, has led to rapid oxidative stress and extensive spinal MN-specific death within a few days [50]. Moreover, oxidative stress induced by a genetic approach specifically in spinal motor neurons in live zebrafish resulted in motor neuron cell death [51]. Thus, it is plausible that reduced protection against oxidative stress by C9-mutated astrocytes, contributes to the gradual loss of motor neurons with age and the eventual onset of the signs and symptoms of fALS. In line with this idea, Edaravone, a free radical scavenger believed to decrease central nervous system oxidative stress was recently approved as a therapy for ALS [39,52,53].

ALS is mainly caused by the specific loss of upper MN (reside in the cortex) and spinal MN. In our study, the toxicity of C9-astrocytic conditioned media was demonstrated on both human spinal cord MN and mouse cortical neurons. While cortical neurons include multiple neuronal cell types in addition to the upper MN, they have been used to model pathology that is specific to ALS [54–56]. In addition, specificity of the non-autonomous astrocytic toxic effect in ALS, may be related to regional-specific properties of the astrocytes. Astrocytes from various anatomical positions in the CNS differ in their transcriptional profile and properties [57]. It has been shown that spinal cord astrocytes express several region-specific genes [58]. One of these genes, Sema3A is encoded only by ventral astrocytes, and in its absence, MNs' survival is reduced [58]. It should be noted that we used an astrocytic differentiation induction protocol which preferably directs toward a ventral spinal cord fate.

One of the cellular responses to oxidative stress is cellular senescence [reviewed in [59]]. Transcriptome analysis in our study

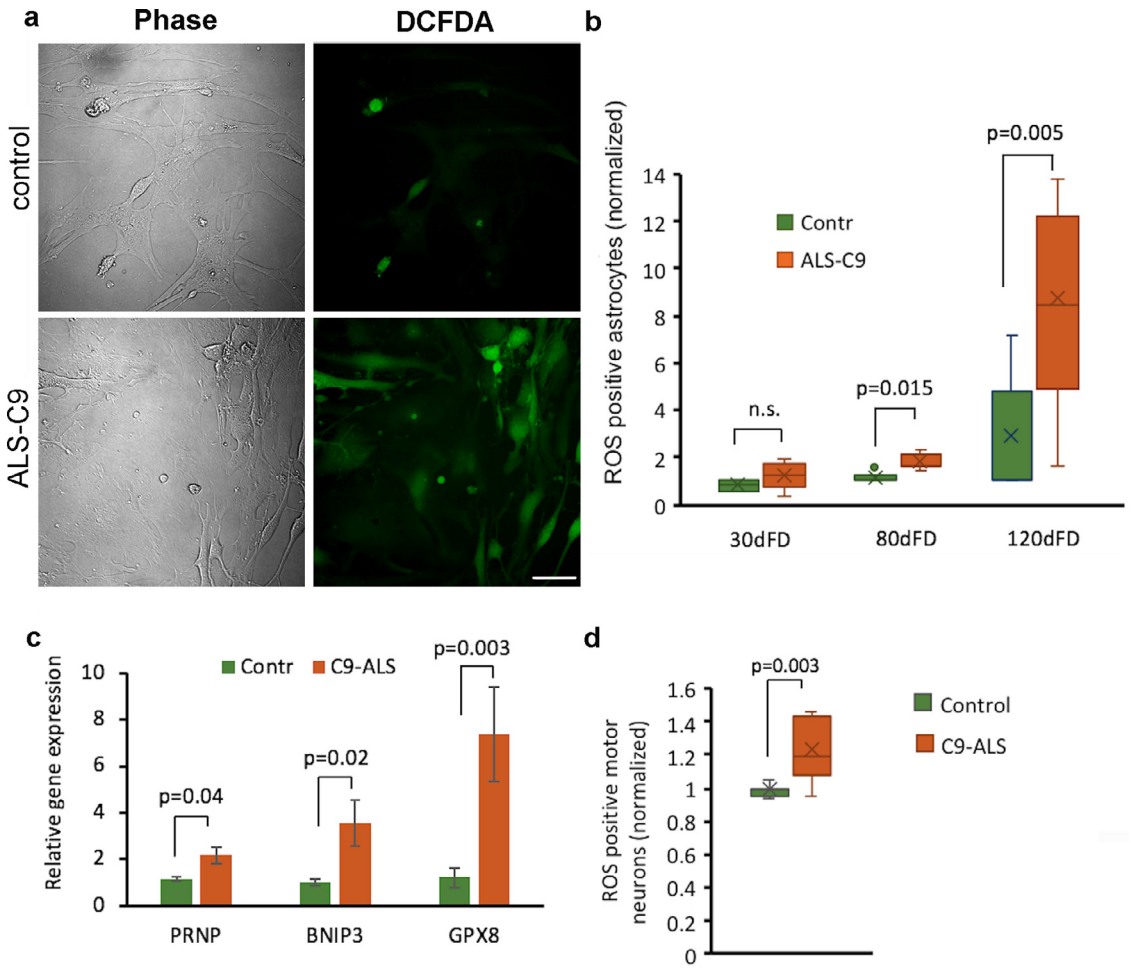

Fig. 7. C9 mutated astrocytes show higher percentage of ROS-positive cells and their secretome can induce higher ROS levels in MNs. (a) Representative phase-contrast and florescence images of control (Contr-L9) and mutated (C9-L8) astrocytes at 90 dFD stained with DCFDA Cellular Reactive Oxygen Species Detection Assay Kit. Scale bar 50 μM. (b) FACS analysis of ROS-positive astrocytes from C9-mutated (C9-L5, C9-L8, C9-L1) and control (Contr-L3, Contr-L9) lines at different time points of FD (30, 80 and 120 dFD). ROS-positive cells were detected by using the DCFDA Cellular Reactive Oxygen Species Detection Assay Kit. Only live cells were counted by exclusion of PI-positive cells. The relative number of ROS-positive cells is presented relative to Contr-L3. Data are presented as a range of values from 3 independent experiments for each time point. (c) qRT-PCR validation of RNA-seq analysis that showed the altered expression of genes related to cellular oxidative stress. RNA was extracted from 4 C9-mutated (C9-L5, C9-L8, C9-L37, C9-L1) and 2 non-mutated (Contr-L3, Contr-L9) astrocyte lines at 80–100 days of FD. Data are presented as mean ± SEM of 3 independent experiments. (d) Oxidative stress of FACS sorted hMNs was analyzed after 8 days in culture in media conditioned by 4 C9-mutated (C9-L5, C9-L8, C9-L37, C9-L1) and 2 non-mutated (Contr-L3, Contr-L9) astrocyte lines at 80–90dFD by using CellROX™ Deep Red Flow Cytometry Assay Kit. Results are expressed as the percent of ROS-positive MNs from live GFP-positive MNs which were gated using PI. Data are presented as a range of values from 4 independent experiments normalized to Contr-L3.

revealed altered senescence-associated pathways in C9-mutated astrocytes, suggesting an increased senescence phenotype of the mutated astrocytes. We validated that indeed, C9-mutated astrocytes acquired the senescence phenotype at a higher rate than control astrocytes. Although senescence in culture does not necessarily represent age-related pathological processes *in vivo*, it is interesting to note that at least in a rodent model of ALS, astrocytes of rats overexpressing a mutant SOD1 obtain a more senescent phenotype than astrocytes of control aged-matched animals [60]. Additionally, the pathological role of senescent cells was suggested in other age-related neurodegenerative disorders, such as Parkinson's disease and Alzheimer's [61,62]. Additional studies are needed to shed light on the contribution of astrocyte senescence to their dysfunction in C9-ALS.

In summary, our data suggest that C9-mutated astrocytes produce and/or release insufficient innate antioxidants, leading to reduced ability to defend not only themselves but also MNs from oxidative stress. We contend this loss of normal astrocytic function underlies cellular injury and neurodegeneration in ALS, and points toward the continued development of therapies aimed at reducing astrocytic and MN oxidative stress in ALS.

Funding sources

This work was kindly supported by a donation from the late Alfred Taubman (B.R. and E.L.F) and the Sinai Medical Staff Foundation (E.L.F), a donation from Judy and Sydney Swartz (B.R.) a grant from Legacy Heritage Biomedical Fund (Grant No. 1306/10, O.B. and B.R.), the Israel Science Foundation Grant No. 947/14, and 401/19 O.B.) and by a research grant from Kadimastem Ltd (B.R.).

Declaration of competing interest

Benjamin Reubinoff is a member of the scientific advisory board of Kadimastem Ltd. and holds options in the company. A major focus of the company is the development of hESC-derived astrocytes for transplantation therapy in ALS. Michal Izrael is an employee of Kadimastem Ltd. and holds options in the company.

Acknowledgments

We are grateful to Dr. Kevin C. Eggan (Department of Stem Cell and Regenerative Biology, Harvard University) for kindly providing

us the HB9-GFP hESC line. We would also like to thank Shelly Tannenbaum for comments on the manuscript. In addition, we thank Dr. Michal Gropp for her professional support. We thank Dr. Gustavo Mostoslavsky for the STEMCCA lentiviral vectors. We thank Crystal Pacut for developing and providing primary fibroblasts from C9-ALS patients and matched healthy controls.

Supplementary materials

Supplementary material associated with this article can be found in the online version at doi:10.1016/j.ebiom.2019.11.026.

References

[1] Gros-Louis F, Gaspar C, Rouleau GA. Genetics of familial and sporadic amyotrophic lateral sclerosis. Biochim Biophys Acta 2006;1762:956–72 https://doi.org/10.1016/j.bbadis.2006.01.004.
[2] Volk AE, Weishaupt JH, Andersen PM, Ludolph AC, Kubisch C. Current knowledge and recent insights into the genetic basis of amyotrophic lateral sclerosis. Med Genet 2018;30:252–8 https://doi.org/10.1007/s11825-018-0185-3.
[3] De Jesus-Hernandez M, Mackenzie IR, Boeve BF, Boxer AL, Baker M, Rutherford NJ, et al. Expanded GGGGCC hexanucleotide repeat in noncoding region of C9ORF72 causes chromosome 9p-linked FTD and ALS. Neuron 2011;72:245–56 https://doi.org/10.1016/j.neuron.2011.09.011.
[4] Renton AE, Majounie E, Waite A, Simón-Sánchez J, Rollinson S, Gibbs JR, et al. A hexanucleotide repeat expansion in C9ORF72 is the cause of chromosome 9p21-linked ALS-FTD. Neuron 2011;72:257–68 https://doi.org/10.1016/j.neuron.2011.09.010.
[5] Fernandez-Fernandez S, Almeida A, Bolaños JP. Antioxidant and bioenergetic coupling between neurons and astrocytes. Biochem J 2012;443:3–11 https://doi.org/10.1042/BJ20111943.
[6] Bélanger M, Allaman I, Magistretti PJ. Brain energy metabolism: focus on astrocyte-neuron metabolic cooperation. Cell Metab 2011;14:724–38 https://doi.org/10.1016/j.cmet.2011.08.016.
[7] Vargas MR, Johnson DA, Johnson JA. Decreased glutathione accelerates neurological deficit and mitochondrial pathology in familial ALS-linked hSOD1(G93A) mice model. Neurobiol Dis 2011;43:543–51 https://doi.org/10.1016/j.nbd.2011.04.025.
[8] Vargas MR, Pehar M, Cassina P, Beckman JS, Barbeito L. Increased glutathione biosynthesis by NrF2 activation in astrocytes prevents p75NTR-dependent motor neuron apoptosis. J Neurochem 2006;97:687–96 https://doi.org/10.1111/j.1471-4159.2006.03742.x.
[9] Clement AM, Nguyen MD, Roberts EA, Garcia ML, Boillée S, Rule M, et al. Wild-type nonneuronal cells extend survival of SOD1 mutant motor neurons in ALS mice. Science 2003;302:113–7 https://doi.org/10.1126/science.1086071.
[10] Di Giorgio FP, Carrasco MA, Siao MC, Maniatis T, Eggan K. Non–cell autonomous effect of glia on motor neurons in an embryonic stem cell–based ALS model. Nat Neurosci 2007;10:608–14 https://doi.org/10.1038/nn1885.
[11] Nagai M, Re DB, Nagata T, Chalazonitis A, Jessell TM, Wichterle H, et al. Astrocytes expressing ALS-linked mutated SOD1 release factors selectively toxic to motor neurons. Nat Neurosci 2007;10:615–22 https://doi.org/10.1038/nn1876.
[12] Marchetto MCN, Muotri AR, Mu Y, Smith AM, Cezar GG, Gage FH. Non-Cell-Autonomous effect of human SOD1G37R astrocytes on motor neurons derived from human embryonic stem cells. Cell Stem Cell 2008;3:649–57 https://doi.org/10.1016/j.stem.2008.10.001.
[13] Yamanaka K, Chun SJ, Boillee S, Fujimori-Tonou N, Yamashita H, Gutmann DH, et al. Astrocytes as determinants of disease progression in inherited ALS. Nat Neurosci 2008;11:251–3 https://doi.org/10.1038/nn2047.
[14] Haidet-Phillips AM, Hester ME, Miranda CJ, Meyer K, Braun L, Frakes A, et al. Astrocytes from familial and sporadic ALS patients are toxic to motor neurons. Nat Biotechnol 2011;29:824–8 https://doi.org/10.1038/nbt.1957.
[15] Meyer K, Ferraiuolo L, Miranda CJ, Likhite S, McElroy S, Renusch S, et al. Direct conversion of patient fibroblasts demonstrates non-cell autonomous toxicity of astrocytes to motor neurons in familial and sporadic ALS. Proc Natl Acad Sci U S A 2014;111:829–32 https://doi.org/10.1073/pnas.1314085111.
[16] Madill M, McDonagh K, Ma J, Vajda A, McLoughlin P, O'Brien T, et al. Amyotrophic lateral sclerosis patient iPSC-derived astrocytes impair autophagy via non-cell autonomous mechanisms. Mol Brain 2017;10:22 https://doi.org/10.1186/s13041-017-0300-4.
[17] Shibata N, Nagai R, Uchida K, Horiuchi S, Yamada S, Hirano A, et al. Morphological evidence for lipid peroxidation and protein glycoxidation in spinal cords from sporadic amyotrophic lateral sclerosis patients. Brain Res. 2001;917:97–104 https://doi.org/10.1016/S0006-8993(01)02926-2.
[18] Pole A, Dimri M, Dimri GP. Oxidative stress, cellular senescence and ageing. Molecular 2016;3:300–24 2016 https://doi.org/10.3934/molsci.2016.3.300.
[19] Das MM, Svendsen CN. Astrocytes show reduced support of motor neurons with aging that is accelerated in a rodent model of ALS. Neurobiol Aging 2015;36:1130–9 https://doi.org/10.1016/j.neurobiolaging.2014.09.020.
[20] Di Giorgio FP, Boulting GL, Bobrowicz S, Eggan KC. Human embryonic stem cell-derived motor neurons are sensitive to the toxic effect of glial cells carrying an ALS-Causing mutation. Cell Stem Cell 2008;3:637–48 https://doi.org/10.1016/j.stem.2008.09.017.
[21] Somers A, Jean J-C, Sommer CA, Omari A, Ford CC, Mills JA, et al. Generation of transgene-free lung disease-specific human induced pluripotent stem cells using a single excisable lentiviral stem cell cassette. Stem Cells 2010;28:1728–40 https://doi.org/10.1002/stem.495.
[22] Mostoslavsky G, Fabian AJ, Rooney S, Alt FW, Mulligan RC. Complete correction of murine Artemis immunodeficiency by lentiviral vector-mediated gene transfer. Proc Natl Acad Sci USA 2006;103:16406–11 https://doi.org/10.1073/pnas.0608130103.
[23] Ben-Dor I, Itsykson P, Goldenberg D, Galun E, Reubinoff BE. Lentiviral vectors harboring a dual-gene system allow high and homogeneous transgene expression in selected polyclonal human embryonic stem cells. Mol Ther 2006;14:255–67 https://doi.org/10.1016/j.ymthe.2006.02.010.
[24] Tannenbaum SE, Turetsky TT, Singer O, Aizenman E, Kirshberg S, Ilouz N, et al. Derivation of xeno-free and GMP-grade human embryonic stem cells–platforms for future clinical applications. PLoS ONE 2012;7:e35325 https://doi.org/10.1371/journal.pone.0035325.
[25] Bilican B, Serio A, Barmada SJ, Nishimura AL, Sullivan GJ, Carrasco M, et al. Mutant induced pluripotent stem cell lines recapitulate aspects of TDP-43 proteinopathies and reveal cell-specific vulnerability. PNAS 2012;109:5803–8 https://doi.org/10.1073/pnas.1202922109.
[26] Serio A, Bilican B, Barmada SJ, Ando DM, Zhao C, Siller R, et al. Astrocyte pathology and the absence of non-cell autonomy in an induced pluripotent stem cell model of TDP-43 proteinopathy. PNAS 2013;110:4697–702 https://doi.org/10.1073/pnas.1300398110.
[27] Somers A, Jean J-C, Sommer CA, Omari A, Ford CC, Mills JA, et al. Generation of transgene-free lung disease-specific human induced pluripotent stem cells using a single excisable lentiviral stem cell cassette. Stem Cells 2010;28:1728–40 https://doi.org/10.1002/stem.495.
[28] Serio A, Bilican B, Barmada SJ, Ando DM, Zhao C, Siller R, et al. Astrocyte pathology and the absence of non-cell autonomy in an induced pluripotent stem cell model of TDP-43 proteinopathy. Proc Natl Acad Sci USA 2013;110:4697–702 https://doi.org/10.1073/pnas.1300398110.
[29] Bilican B, Serio A, Barmada SJ, Nishimura AL, Sullivan GJ, Carrasco M, et al. Mutant induced pluripotent stem cell lines recapitulate aspects of TDP-43 proteinopathies and reveal cell-specific vulnerability. Proc Natl Acad Sci USA 2012;109:5803–8 https://doi.org/10.1073/pnas.1202922109.
[30] Chambers SM, Fasano CA, Papapetrou EP, Tomishima M, Sadelain M, Studer L. Highly efficient neural conversion of human ES and iPS cells by dual inhibition of SMAD signaling. Nat Biotechnol 2009;27:275–80 https://doi.org/10.1038/nbt.1529.
[31] Wichterle H, Lieberam I, Porter JA, Jessell TM. Directed differentiation of embryonic stem cells into motor neurons. Cell 2002;110:385–97.
[32] Li X-J, Du Z-W, Zarnowska ED, Pankratz M, Hansen LO, Pearce RA, et al. Specification of motoneurons from human embryonic stem cells. Nat Biotechnol 2005;23:215–21 https://doi.org/10.1038/nbt1063.
[33] Nihei K, McKee AC, Kowall NW. Patterns of neuronal degeneration in the motor cortex of amyotrophic lateral sclerosis patients. Acta Neuropathol 1993;86:55–64.
[34] Agosta F, Valsasina P, Riva N, Copetti M, Messina MJ, Prelle A, et al. The cortical signature of amyotrophic lateral sclerosis. PLoS ONE 2012;7:e42816 https://doi.org/10.1371/journal.pone.0042816.
[35] Lee H, Shamy GA, Elkabetz Y, Schofield CM, Harrsion NL, Panagiotakos G, et al. Directed differentiation and transplantation of human embryonic stem cell-derived motoneurons. Stem Cells 2007;25:1931–9 https://doi.org/10.1634/stemcells.2007-0097.
[36] Ben-Shushan E, Feldman E, Reubinoff BE. Notch signaling regulates motor neuron differentiation of human embryonic stem cells. Stem Cells 2014;33:403–15 https://doi.org/10.1002/stem.1873.
[37] Bhat R, Crowe EP, Bitto A, Moh M, Katsetos CD, Garcia FU, et al. Astrocyte senescence as a component of Alzheimer's disease. PLoS ONE 2012;7:e45069 https://doi.org/10.1371/journal.pone.0045069.
[38] Bitto A, Sell C, Crowe E, Lorenzini A, Malaguti M, Hrelia S, et al. Stress-induced senescence in human and rodent astrocytes. Exp. Cell Res. 2010;316:2961–8 https://doi.org/10.1016/j.yexcr.2010.06.021.
[39] Van Brussel I, Schrijvers DM, Martinet W, Pintelon I, Deschacht M, Schnorbusch K, et al. Transcript and protein analysis reveals better survival skills of monocyte-derived dendritic cells compared to monocytes during oxidative stress. PLoS ONE 2012;7:e43357 https://doi.org/10.1371/journal.pone.0043357.
[40] Ramming T, Hansen HG, Nagata K, Ellgaard L, Appenzeller-Herzog C. GPx8 peroxidase prevents leakage of H_2O_2 from the endoplasmic reticulum. Free Radical Biology and Medicine 2014;70:106–16 https://doi.org/10.1016/j.freeradbiomed.2014.01.018.
[41] Schmidt A, von Woedtke T, Bekeschus S. Periodic exposure of keratinocytes to cold physical plasma: an in vitro model for redox-related diseases of the skin. Oxid Med Cell Longev 2016 https://doi.org/10.1155/2016/9816072.
[42] Barber SC, Mead RJ, Shaw PJ. Oxidative stress in ALS: a mechanism of neurodegeneration and a therapeutic target. Biochimica et Biophysica Acta (BBA) - Molecular Basis of Disease 2006;1762:1051–67 https://doi.org/10.1016/j.bbadis.2006.03.008.
[43] Cassina P, Cassina A, Pehar M, Castellanos R, Gandelman M, de León A, et al. Mitochondrial dysfunction in SOD1G93A-bearing astrocytes promotes motor neuron degeneration: prevention by mitochondrial-targeted antioxidants. J Neurosci 2008;28:4115–22 https://doi.org/10.1523/JNEUROSCI.5308-07.2008.
[44] Almad AA, Doreswamy A, Gross SK, Richard J-P, Huo Y, Haughey N, et al. Connexin 43 in astrocytes contributes to motor neuron toxicity in amyotrophic lateral sclerosis. Glia 2016;64:1154–69 https://doi.org/10.1002/glia.22989.
[45] Ferraiuolo L, Kirby J, Grierson AJ, Sendtner M, Shaw PJ. Molecular pathways of motor neuron injury in amyotrophic lateral sclerosis. Nat Rev Neurol 2011;7:616–30 https://doi.org/10.1038/nrneurol.2011.152.

[46] Sasaki S, Warita H, Abe K, Iwata M. Inducible nitric oxide synthase (iNOS) and nitrotyrosine immunoreactivity in the spinal cords of transgenic mice with a G93A mutant SOD1 gene. J Neuropathol Exp Neurol 2001;60:839–46.
[47] Aoki Y, Manzano R, Lee Y, Dafinca R, Aoki M, Douglas AGL, et al. C9orf72 and RAB7L1 regulate vesicle trafficking in amyotrophic lateral sclerosis and frontotemporal dementia. Brain 2017;140:887–97 https://doi.org/10.1093/brain/awx024.
[48] Varcianna A, Myszczynska MA, Castelli LM, O'Neill B, Kim Y, Talbot J, et al. Micro-RNAs secreted through astrocyte-derived extracellular vesicles cause neuronal network degeneration in C9orf72 als. EBioMedicine 2019;40:626–35 https://doi.org/10.1016/j.ebiom.2018.11.067.
[49] Lopez-Gonzalez R, Lu Y, Gendron TF, Karydas A, Tran H, Yang D, et al. Poly(GR) in C9ORF72-Related ALS/FTD compromises mitochondrial function and increases oxidative stress and DNA damage in iPSC-Derived motor neurons. Neuron 2016;92:383–91 https://doi.org/10.1016/j.neuron.2016.09.015.
[50] Rojas F, Cortes N, Abarzua S, Dyrda A, van Zundert B. Astrocytes expressing mutant SOD1 and TDP43 trigger motoneuron death that is mediated via sodium channels and nitroxidative stress. Front Cell Neurosci 2014;8:24 https://doi.org/10.3389/fncel.2014.00024.
[51] Formella I, Svahn AJ, Radford RAW, Don EK, Cole NJ, Hogan A, et al. Real-time visualization of oxidative stress-mediated neurodegeneration of individual spinal motor neurons *in vivo*. Redox Biol 2018;19:226–34 https://doi.org/10.1016/j.redox.2018.08.011.
[52] Takei K, Watanabe K, Yuki S, Akimoto M, Sakata T, Palumbo J. Edaravone and its clinical development for amyotrophic lateral sclerosis. Amyotrophic Lateral Sclerosis and Frontotemporal Degeneration 2017;18:5–10 https://doi.org/10.1080/21678421.2017.1353101.
[53] Cruz MP. Edaravone (Radicava) A Novel Neuroprotective Agent for the Treatment of Amyotrophic Lateral SclerosisMartin Paspe Cruz. P&T Community 2018;43:25–8.
[54] TDP-43 causes neurotoxicity and cytoskeletal dysfunction in primary cortical neurons n.d. https://journals.plos.org/plosone/article?id=10.1371/journal.pone.0196528 (accessed October 15, 2019).
[55] Commisso B, Ding L, Varadi K, Gorges M, Bayer D, Boeckers TM, et al. Stage-dependent remodeling of projections to motor cortex in ALS mouse model revealed by a new variant retrograde-AAV9. Elife 2018;7:e36892 https://doi.org/10.7554/eLife.36892.
[56] Westergard T, McAvoy K, Russell K, Wen X, Pang Y, Morris B, et al. Repeat-associated non-AUG translation in C9orf72-ALS/FTD is driven by neuronal excitation and stress. EMBO Mol Med 2019;11 https://doi.org/10.15252/emmm.201809423.
[57] Miller SJ. Astrocyte heterogeneity in the adult central nervous system. Front Cell Neurosci 2018;12 https://doi.org/10.3389/fncel.2018.00401.
[58] Molofsky AV, Kelley KW, Tsai H-H, Redmond SA, Chang SM, Madireddy L, et al. Astrocyte-encoded positional cues maintain sensorimotor circuit integrity. Nature 2014;509:189–94 https://doi.org/10.1038/nature13161.
[59] Pole A, Dimri M, Dimri GP. Oxidative stress, cellular senescence and ageing. Molecular 2016;3:300–24 https://doi.org/10.3934/molsci.2016.3.300.
[60] Das MM, Svendsen CN. Astrocytes show reduced support of motor neurons with aging that is accelerated in a rodent model of ALS. Neurobiol Aging 2015;36:1130–9 https://doi.org/10.1016/j.neurobiolaging.2014.09.020.
[61] Chinta SJ, Woods G, Demaria M, Rane A, Zou Y, McQuade A, et al. Cellular senescence is induced by the environmental neurotoxin paraquat and contributes to neuropathology linked to Parkinson's disease. Cell Rep 2018;22:930–40 https://doi.org/10.1016/j.celrep.2017.12.092.
[62] Bussian TJ, Aziz A, Meyer CF, Swenson BL, Deursen JM, Baker DJ. Clearance of senescent glial cells prevents tau-dependent pathology and cognitive decline. Nature 2018;562:578 https://doi.org/10.1038/s41586-018-0543-y.